2000-12-01

Dynamics of signaling between Ca(2+) sparks and Ca(2+)-activated K(+) channels studied with a novel image-based method for direct intracellular measurement of ryanodine receptor Ca(2+) current

Ronghua ZhuGe
University of Massachusetts Medical School

Et al.

Published November 29, 2000

Dynamics of Signaling between Ca^{2+} Sparks and Ca^{2+}- activated K^+ Channels Studied with a Novel Image-based Method for Direct Intracellular Measurement of Ryanodine Receptor Ca^{2+} Current

RONGHUA ZHUGE,*‡ KEVIN E. FOGARTY,*‡ RICHARD A. TUFT,*‡ LAWRENCE M. LIFSHITZ,*‡ KEMAL SAYAR,‡ and JOHN V. WALSH JR.‡

From the *Biomedical Imaging Group and ‡Department of Physiology, University of Massachusetts Medical School, Worcester, Massachusetts 01655

ABSTRACT Ca^{2+} sparks are highly localized cytosolic Ca^{2+} transients caused by a release of Ca^{2+} from the sarcoplasmic reticulum via ryanodine receptors (RyRs); they are the elementary events underlying global changes in Ca^{2+} in skeletal and cardiac muscle. In smooth muscle and some neurons, Ca^{2+} sparks activate large conductance Ca^{2+}-activated K^+ channels (BK channels) in the spark microdomain, causing spontaneous transient outward currents (STOCs) that regulate membrane potential and, hence, voltage-gated channels. Using the fluorescent Ca^{2+} indicator fluo-3 and a high speed widefield digital imaging system, it was possible to capture the total increase in fluorescence (i.e., the signal mass) during a spark in smooth muscle cells, which is the first time such a direct approach has been used in any system. The signal mass is proportional to the total quantity of Ca^{2+} released into the cytosol, and its rate of rise is proportional to the Ca^{2+} current flowing through the RyRs during a spark ($I_{Ca(spark)}$). Thus, Ca^{2+} currents through RyRs can be monitored inside the cell under physiological conditions. Since the magnitude of $I_{Ca(spark)}$ in different sparks varies more than fivefold, Ca^{2+} sparks appear to be caused by the concerted opening of a number of RyRs. Sparks with the same underlying Ca^{2+} current cause STOCs, whose amplitudes vary more than threefold, a finding that is best explained by variability in coupling ratio (i.e., the ratio of RyRs to BK channels in the spark microdomain). The time course of STOC decay is approximated by a single exponential that is independent of the magnitude of signal mass and has a time constant close to the value of the mean open time of the BK channels, suggesting that STOC decay reflects BK channel kinetics, rather than the time course of $[Ca^{2+}]$ decline at the membrane. Computer simulations were carried out to determine the spatiotemporal distribution of the Ca^{2+} concentration resulting from the measured range of $I_{Ca(spark)}$. At the onset of a spark, the Ca^{2+} concentration within 200 nm of the release site reaches a plateau or exceeds the $[Ca^{2+}]_{EC50}$ for the BK channels rapidly in comparison to the rate of rise of STOCs. These findings suggest a model in which the BK channels lie close to the release site and are exposed to a saturating $[Ca^{2+}]$ with the rise and fall of the STOCs determined by BK channel kinetics. The mechanism of signaling between RyRs and BK channels may provide a model for Ca^{2+} action on a variety of molecular targets within cellular microdomains.

KEY WORDS: widefield digital microscope • sarcoplasmic reticulum • microdomain • STOC • smooth muscle release

INTRODUCTION

Calcium ions, which serve as signals for a wide range of cellular processes, can enter the nucleus and cytosol either from outside the cell or from the endoplasmic reticulum/sarcoplasmic reticulum. Two types of Ca^{2+} release channels mediate release from the endoplasmic reticulum/sarcoplasmic reticulum.; ryanodine receptors (RyRs)[1] and inositol 1,4,5-trisphosphate receptors. The activation of inositol 1,4,5-trisphosphate receptors or RyRs generates highly localized Ca^{2+} transients, called "Ca^{2+} puffs" and "Ca^{2+} sparks," respectively (Parker and Yao, 1991; Cheng et al., 1993). In many cases these constitute the elementary building blocks underlying global increases in intracellular Ca^{2+} concentration ($[Ca^{2+}]_i$). In addition, these transients can function as signals that achieve specificity by activating targets solely in the vicinity of the release, i.e., targets that are colocalized with the release sites in a microdomain. A possible consequence of such proximity is that a target with relatively low affinity for Ca^{2+} will respond only to local Ca^{2+} release and remain protected from global Ca^{2+} elevations of lower amplitude. Hence, an analysis of the functional and spatial relationship between localized Ca^{2+} transients and their targets is critical for understanding the specificity of Ca^{2+} signaling.

R. ZhuGe and K.E. Fogarty contributed equally to this work.

Address all correspondence to John V. Walsh Jr., Department of Physiology, University of Massachusetts Medical Center, Worcester, MA 01655-027. Fax: (508) 856-5997; E-mail: john.walsh@umassmed.edu

[1]*Abbreviations used in this paper:* BK channel, large conductance Ca^{2+}-activated K^+ channel; FWHM, full width at half maximum; PSF, point spread function; RyR, ryanodine receptor; $I_{(Ca)spark}$, Ca^{2+} spark Ca^{2+} current; STOC, spontaneous transient outward current; TTP, time to peak.

Published November 29, 2000

Smooth muscle cells provide an especially useful system to study the relationship between local Ca^{2+} release events and targets within their microdomains because at least two of the targets are ion channels that are readily monitored at high temporal resolution with patch-clamp recording. In smooth muscle cells, Ca^{2+} sparks induce spontaneous transient outward currents (STOCs) by activating Ca^{2+}-activated K^+ channels (Nelson et al., 1995; Mironneau et al., 1996; Bolton and Gordienko, 1998; ZhuGe et al., 1998, 1999) as well as spontaneous transient inward currents by opening Ca^{2+}-activated Cl^- channels (ZhuGe et al., 1998). Because the STOCs are blocked by iberiotoxin and their activation is voltage sensitive, it has been concluded that large conductance Ca^{2+}-activated K^+ channels (BK channels) underlie the STOCs (Nelson et al., 1995; ZhuGe et al., 1999). Interest in STOCs has heightened since the pioneering work of Nelson et al. (1995; see also Brenner et al., 2000), which provided strong evidence that STOCs regulate vascular tone in cerebral arteries. Hence, the underlying Ca^{2+} sparks have an important physiological role in their own right, in contrast to serving simply as building blocks for global elevations in Ca^{2+}. Similarly, ZhuGe et al. (1998) have suggested that sparks generating spontaneous transient inward currents regulate contractility in airway smooth muscle.

Studies of the quantitative relationship between Ca^{2+} sparks and STOCs have focused largely on establishing and corroborating the causal link between them (Nelson et al., 1995; Mironneau et al., 1996; Bolton and Gordienko, 1998; ZhuGe et al., 1998, 1999; Perez et al., 1999). However, the mechanisms by which the STOC is generated and the nature of the functional relationship between RyRs and BK channels in the spark microdomain have not been established in detail. For example, do one or more RyRs contribute to a spark? To what degree do the local $[Ca^{2+}]$, the kinetics of the underlying Ca^{2+} flux through the RyRs, and the kinetics of BK channel gating determine the spark–STOC relationship? In the present mechanistic study, we address questions of this sort.

To date, studies of Ca^{2+} sparks have measured changes in fluorescence relative to background (F/F_0 or $100 \times (F - F_0)/F_0$), usually with fluo-3, as an index of alterations in Ca^{2+} concentration. In the present study, we use a measure of the quantity of Ca^{2+} released during a spark, a measure similar to the signal mass unit that Sun et al. (1998) devised to analyze Ca^{2+} puffs in oocytes. Using a confocal linescan system, Sun et al. (1998) measured F/F_0 in the usual way and computed the total fluorescence based on a model of the extent of the puff. In the present study, we have developed a new method for the direct measure of the total increase in fluorescence due to entry of Ca^{2+} into the cytosol. This is made possible by the use of a widefield digital imaging system that can capture the increase in fluorescence over a sufficiently large volume and with sufficiently low noise to allow detection of the total increase in fluorescence because of a localized rise in cytosolic Ca^{2+}.

The present study is the first application of a direct signal mass approach to the study of Ca^{2+} sparks in any system. The use of the signal mass approach affords three advantages. First, since this measure discloses the total Ca^{2+} released (i.e., the integrated flux) over a known time, the Ca^{2+} flux or, in terms of charge, the Ca^{2+} current through the RyRs during a spark (i.e., $I_{Ca(spark)}$) can be determined. Second, it is uncertain whether fluorescent indicators are capable of reporting the $[Ca^{2+}]$ in the microdomain, where the BK channels underlying a STOC reside, since equilibrium conditions between released Ca^{2+} and indicator may not be reached there (Stern, 1992; Naraghi and Neher, 1997). Hence, an uncertain measure of concentration can be replaced by a measure of the signal mass and Ca^{2+} flux or current, which can be related to the STOCs. Third, using two-dimensional widefield imaging, as was done in this study, the signal mass is essentially independent of the z-axis location of the spark relative to the microscope's plane of focus.

Major results of the present study are as follows. First, most sparks result from the concerted opening of a number of RyRs. Second, 21% of sparks fail to cause detectable STOCs. Third, a given $I_{Ca(spark)}$ leads to STOCs of different magnitude because of, at least in part, different ratios of RyRs to BK channels in the spark microdomains. Fourth, the rate of STOC activation is relatively constant in the face of large differences in $I_{Ca(spark)}$. Fifth, STOC decay is approximated by a single exponential function that is independent of the magnitude of the Ca^{2+} signal mass and close to the value of the mean open time of the BK channels at the same potential. These findings suggest a model of the STOC in which the spark presents to the BK channels a step increase in $[Ca^{2+}]$ to levels well above the EC_{50} for the BK channels. In this model, the rise and fall of the STOC is determined by the kinetics of the BK channels and not by diffusion of Ca^{2+} to the BK channels or by the rate of rise or fall of $[Ca^{2+}]_i$. The signal mass approach coupled with widefield microscopy should provide insights into focal Ca^{2+} transients elsewhere, for example, in striated muscle or in dendritic spines of neurons.

MATERIALS AND METHODS

Preparation of Cells and Patch-Clamp Recording

Single smooth muscle cells were enzymatically dispersed from the stomach muscularis of *Bufo marinus* as described previously (Fay et al., 1982). Membrane currents were recorded using the tight-seal, whole-cell patch recording configuration. The extracellular solution contained (in mM): 130 NaCl, 3 KCl, 1.8 $CaCl_2$, 1 $MgCl_2$, 10 HEPES, and the pH was adjusted to 7.4 with NaOH.

Published November 29, 2000

The pipet solution contained the following (in mM): 137 KCl, 3 $MgCl_2$, 10 HEPES, 3 Na_2ATP, 0.05 fluo-3 (unless otherwise noted), and the pH was adjusted to 7.2 with KOH. All experiments were carried out at room temperature. Whole-cell currents were recorded and low pass–filtered using the Axopatch 1D amplifier (200-Hz cutoff) and digitally sampled at 1 kHz or, in some instances, the Axoclamp 2A amplifier (100-Hz cutoff, then digitally sampled at 300 Hz), and stored for analysis. Events were counted as STOCs if they exceeded a threshold of 10 pA, as detected by a custom-automated algorithm that also measured their amplitude and frequency. The events were checked by visual inspection to eliminate anomalies such as multiple events overlapping in time or excessively noisy traces.

Detection and Measurement of Ca^{2+} Sparks

The following two measures of Ca^{2+} sparks were used: the conventional fluorescence ratio, $\Delta F/F_0$; and the change in total fluorescence $F^T - F_0^T$, which is related to the total Ca^{2+} released into the cytosol, also termed the signal mass. The two measures differ not only in the way they are computed, but also in the area from which the fluorescence is collected. The ratio measure is tracked for a single pixel, whereas the signal mass is collected over a much larger area. For each measure, fluorescent images were obtained using fluo-3 as the calcium indicator and a custom built widefield, high speed digital imaging system that is described in detail elsewhere (ZhuGe et al., 1999). Rapid imaging was made possible by using a cooled high sensitivity, charge-coupled device camera (128 × 128 pixels) developed in conjunction with MIT Lincoln Laboratories. The camera was interfaced to a custom-made, inverted microscope equipped with a 40× oil immersion lens (NA 1.3); each pixel covered a 333 × 333-nm area of the cell. The 488-nm line of a multiline Argon laser provided fluorescence excitation for the indicator fluo-3. Emission of the Ca^{2+} indicator was imaged at wavelengths >500 nm. To obtain a constant concentration of Ca^{2+} indicator, 50 μM fluo-3 was delivered through the patch pipet, and measurements were not commenced until 10–15 min after breakthrough of the patch. After this time, no significant change in background fluorescence was detected. Subsequent image processing and analysis were performed off-line using a custom-designed software package, running on a Silicon Graphics workstation.

Fluorescence Ratio

For this measure, the fluo-3 images were first smoothed by convolution with a 3 × 3-pixel approximation to a two-dimensional Gaussian:

$$\begin{bmatrix} \frac{1}{16} & \frac{2}{16} & \frac{1}{16} \\ \frac{2}{16} & \frac{4}{16} & \frac{2}{16} \\ \frac{1}{16} & \frac{2}{16} & \frac{1}{16} \end{bmatrix}.$$

Fluorescence ratio images were calculated and expressed as a percentage on a pixel to pixel basis from the equation:

$$\Delta F/F_0(\%) = 100 \times (F - F_0)/F_0 = 100 \times \frac{(F(x, y, t) - F_0(x, y))}{F_0(x,y)}, \quad (1)$$

where F is the fluorescence at each pixel in the time series, and F_0 is the resting level derived from the fluorescence time series by computing the median pixel value during quiescent times at each F(x, y). The $\Delta F/F_0$ traces in the figures follow the time course of the single pixel that had the highest fluorescence ratio, which we call the epicenter pixel. For an event to qualify as a Ca^{2+} spark, it had to meet two criteria. First, the fluorescence ratio at the epicenter pixel had to be equal to or >5%, and it had to last for at least two consecutive time frames of 10 ms. The second criterion was based on the signal mass, which is described in detail in the next section.

Ca^{2+} Quantity or Signal Mass

During a spark, free Ca^{2+} (diffusion coefficient, D = 250 $\mu m^2/s$) and Ca^{2+} bound to fluo-3 (D = 22 $\mu m^2/s$; Smith et al., 1998) quickly diffuse away from the spark release site as Ca^{2+} continues to be discharged. To quantify the total fluorescence arising from the binding of fluo-3 to the discharged Ca^{2+}(i.e., the Ca^{2+} signal mass), the increase in fluo-3 fluorescence) must be collected from a sufficiently large volume to provide a measure of the total quantity of Ca^{2+} released. Custom software was used to process the images and extract signal mass information for each spark event. The signal mass time course for each spark was computed from the two-dimensional, widefield fluorescence images of fluo-3 according to the following equations.

Total fluorescence,

$$F^T(t) = \sum_{\Delta x = -20}^{+20} \sum_{\Delta y = -20}^{+20} F(x + \Delta x, y + \Delta y, t). \quad (2)$$

The fluorescence F is summed over a 13.7-μm square region (41 pixels on a side in the x-y plane) surrounding the spark epicenter pixel (x,y) as determined from the $\Delta F / F_0$ images from Eq. 1.

Signal mass,

$$sm(t) = G(F^T(t) - F^T(t_0)). \quad (3)$$

The signal mass sm(t) is the change in total fluorescence $F^T(t)$ over the baseline fluorescence $F^T(t_0)$ times the detector gain G (see below). The time t_0 corresponds to the image immediately preceding the beginning of the spark. The beginning of the spark event was identified as the first image having a flux, i.e., an increase in total fluorescence (F^T) relative to the preceding image, exceeding 2 SDs of the noise in the flux measurement, which were calculated according to the following equations:

Pixel noise,

$$\sigma(x, y, t) = \sqrt{(G \cdot F(x, y, t)) + N^2}. \quad (4)$$

Total noise,

$$\sigma^T(t) = \sqrt{\sum_{\Delta x = -20}^{+20} \sum_{\Delta y = -20}^{+20} \sigma(x + \Delta x, y + \Delta y, t)^2}. \quad (5)$$

Fluorescence flux,

$$flux(t) = \frac{G \cdot (F^T(t) - F^T(t - \Delta t))}{\Delta t}. \quad (6)$$

Flux noise,

$$\sigma_{flux}(t) = \frac{\sqrt{\sigma^T(t)^2 + \sigma^T(t - \Delta t)^2}}{\Delta t}. \quad (7)$$

Spark threshold,

$$flux(t) \geq 2 \cdot \sigma_{flux}(t). \quad (8)$$

(Note that the flux is proportional to the Ca^{2+} current through the RyRs, and the signal mass is proportional to the integrated Ca^{2+} current or total charge carried by Ca^{2+} during the spark. See Eqs. 9 and 10.) The high speed CCD camera was previously

Published November 29, 2000

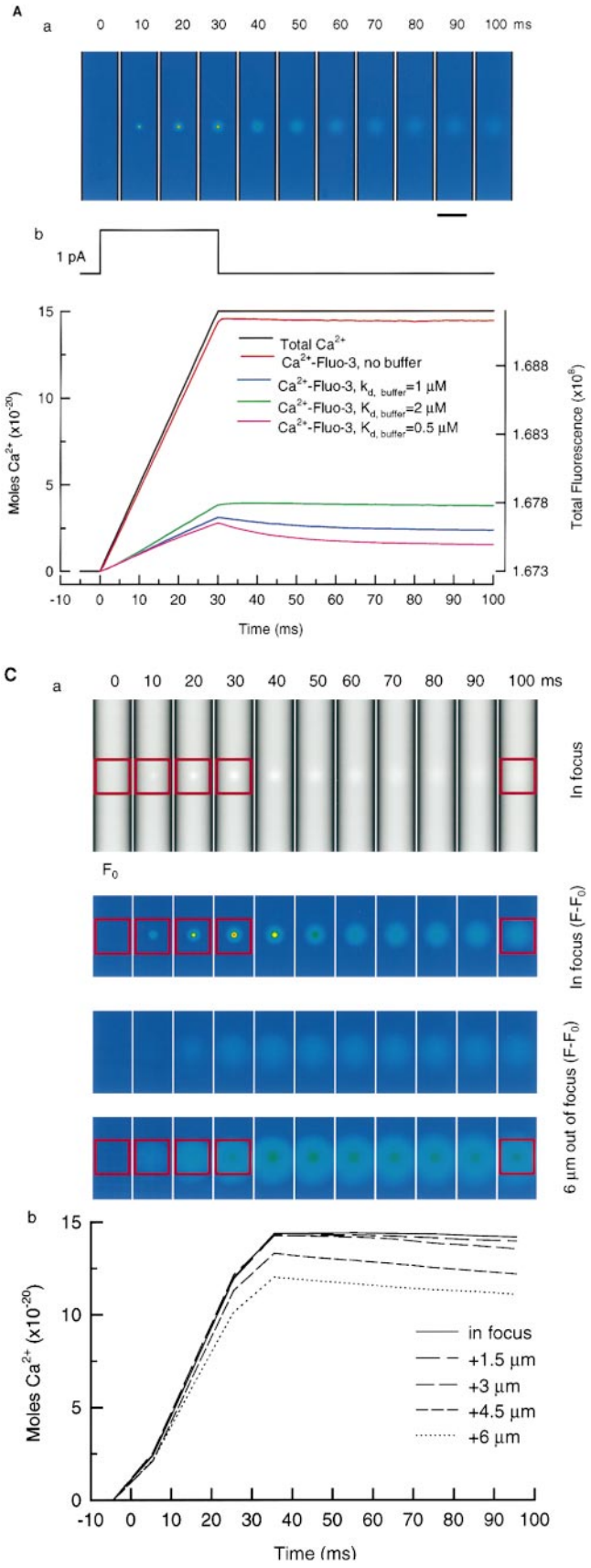

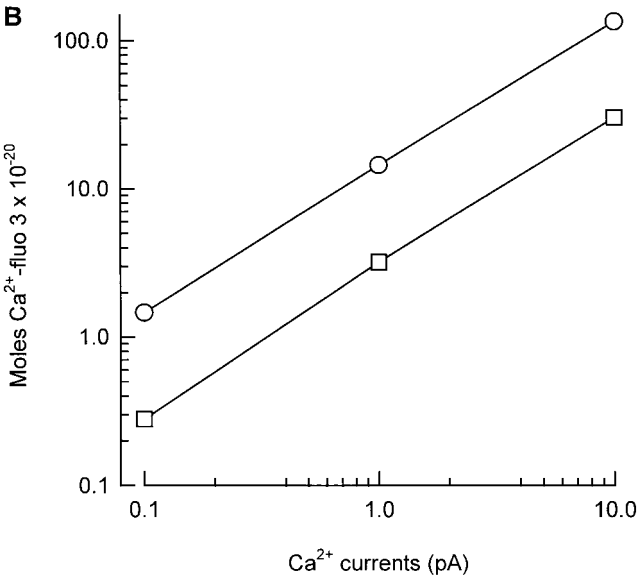

FIGURE 1. Computer simulation of Ca^{2+} entry into the cytosol reveals that the increase in total fluo-3 fluorescence (i.e., signal mass) is a reliable indicator of the total quantity of Ca^{2+} released. (A) Reaction–diffusion kinetics of fluo-3 were simulated in response to a Ca^{2+} current (1 pA in magnitude and 30 ms in duration; top panel of b) from a point source into the center of a cylindrical model cell with a diameter of 12 μm. a shows the evolution of a continuous series of simulated 10-ms fluorescence images. The bottom panel of b shows the integrated Ca^{2+}, i.e., the signal mass (black line), and the total increase in fluorescence emitted from Ca^{2+}-bound fluo-3 under various conditions: in the absence of fixed buffers (red line) and in the presence of 230-μM fixed Ca^{2+} buffer with a K_d of 0.5 μM (pink line), 1 μM (blue line), or 2 μM (green line). (In each case, the fixed buffer has the same k_{on}, appropriate for diffusion limitation and varying k_{off}'s.) Note that, in the absence of fixed buffer, fluo-3 fluorescence closely follows the change of total Ca^{2+} from the source, suggesting that most of the Ca^{2+} ions are bound to fluo-3; and that fixed buffers proportionally decrease fluo-3 fluorescence as their K_d increases. Parameters used for simulations are as follows: basal Ca^{2+} concentration of 0.1 μM; total fluo-3 concentration of 50 μM and total endogenous fixed buffer concentration of 230 μM; an on-rate of 8×10^{-7} $M^{-1}s^{-1}$ for fluo-3 and 10^{-8} $M^{-1}s^{-1}$ for fixed buffer; an off-rate of 90 s^{-1} for fluo-3 and 50, 100, 200 s^{-1} for fixed buffer (yielding a K_d of 1.1 μM for fluo-3 and 2, 1, 0.5 μM, respectively, for fixed buffers); a diffusion constant of 250 $\mu m^2 s^{-1}$ for Ca^{2+} and 22 $\mu m^2 s^{-1}$ for free fluo-3. (B) Results of simulations like the ones in Fig. 1 A, showing the amount of Ca^{2+} bound to fluo-3 at the end of a 30-ms pulse of a range of Ca^{2+} currents. For each level of Ca^{2+} current, the rise was linear with time as in Fig. 1 A. Top line (circles) gives the result in the presence of 50 μM fluo-3 alone, and the bottom line (squares) gives the result in the presence of both fluo-3 and 230 μM of 0.5 μM K_d fixed buffer illustrated in Fig. 1 A. This plot provides a calibration for the signal mass for a wide range of Ca^{2+} currents. (C) The measure of signal mass based on the wide-field microscope accounts for nearly all the fluorescence, whether the spark release site is in or out of focus. The fluorescence generated by the simulation shown in A was blurred in three dimensions using a PSF that was determined empirically as explained in Carrington et al. (1995). The result is shown in the top row of a; note that this simulation is for a spark whose epicenter lies in the plane of microscope focus. The second row from the top displays the fluorescence above baseline for the data in the first row. The third row displays the fluorescence when the spark epicenter is out of focus at the same gain as the second row. The bottom row displays the same

Published November 29, 2000

calibrated as having a linear response to light with a gain (G) of five detected photons per digital count and an RMS readout noise (N) equivalent to five detected photons at each pixel. In Eqs. 6 and 7, $\Delta t = 10$ ms is the time between two consecutive images. Eq. 8 defines the threshold Ca^{2+} flux required to be considered as a spark. Therefore, t_0 refers to the image immediately before the first significant flux is observed. The end of the spark event was taken as the last consecutive image having a significant change in total fluorescence, using the same criterion as for the beginning of the event. Finally, the peak signal mass was calculated as the difference in the total fluorescence between the end image and that preceding the beginning of the event. Since the total noise depends on the absolute fluorescence of the pixels in the image, the threshold noise level may vary from spark to spark.

With a widefield imaging system, photons emitted from fluo-3 molecules both at the plane of focus and outside of it are collected by the optics and imaged onto the camera. Clearly, not all the sparks detected will be centered in the plane of focus, and so the fluorescence from them will not be focused as sharply on the CCD camera, but appear as a blur and hence occupy a larger area. Thus, the area of collection must be large enough so that a negligible fraction of photons from an out of focus spark escape detection. In addition, the area of collection must be large enough to allow for the diffusional spread of Ca^{2+} and Ca^{2+} bound to fluo-3. The size of the area for the measurement was chosen by expanding the area around the epicenter for each spark in the entire data set by increments of 4 pixels on a side. The mean value of the signal mass for the spark population began to level off for areas larger than 17×17 pixels, and further increase was negligible for areas larger than 41×41 pixels. A larger area was not used to avoid decreasing the signal to noise ratio; i.e., the total noise (σ^T) in Eq. 5 increases with an increase in measurement area, whereas the signal mass in Eq. 3 only increases if additional discharged Ca^{2+} is encompassed. To validate this empirical choice, we also used simulations as described in the next section.

We recorded a total of 365 local Ca^{2+} transients in 31 cells that met the criteria for a Ca^{2+} spark as defined above. Of these, 75 generated no STOCs; 110 generated STOCs where measurement of amplitude was uncertain because of contamination by other STOCs or noise in the records; and 180 generated STOCs whose amplitude was clearly measurable. Of these 180 sparks, 34 had STOCs with noise in the current trace at their onset, which made it impossible to determine the time point of STOC initiation. Thus, 146 sparks with their corresponding STOCs were used to determine the spark–STOC relation based on signal averaging as shown in Figs. 5 and 9. In addition, we recorded 2,348 STOCs in 15 additional cells in the absence of fluo-3 in the pipet for the comparison made in Fig. 6.

Calibration of Signal Mass into Moles of Ca^{2+}

To obtain a calibration factor for converting fluorescence to quantity of Ca^{2+}, we used the resting or basal fluorescence since the resting $[Ca^{2+}]$ in these cells is accurately known from earlier studies using fura-2 (Drummond and Fay, 1996). We first determined the fluorescence, or photon count, due to the resting $[Ca^{2+}]$ as follows. Basal fluo-3 fluorescence emanating from a volume subtended by a 5.67-μm (17×17 pixels) square area about each spark epicenter pixel was measured just before each spark in the data set. The mean basal fluorescence for the entire population was determined to be 2.73×10^5 detected photons. Given a total fluo-3 concentration of 50 μM, $K_d = 1.1$ μM (Harkins et al., 1993) and equilibrium with a resting $[Ca^{2+}]$ of 100 nM, the concentration of Ca^{2+}-bound fluo-3 in the cells was 4.08 μM, and the Ca^{2+}-free fluo-3 was 45.92 μM. Given that Ca^{2+}-bound fluo-3 is 200 times brighter than the Ca^{2+}-free, the Ca^{2+}-bound fluo-3 contributed 94.7% of the basal fluorescence. The basal fluorescence due to just the Ca^{2+} bound fluo-3 was therefore 2.58×10^5 detected photons.

Since photons emitted from fluo-3 molecules both at the plane of focus and outside of it are collected by the optics and imaged onto the camera, the actual imaged volume subtended by the 5.67 μm square measurement area must be calculated. We assume that sparks occur at random across the two-dimensional image of the cell, and the average of the cell thickness at all possible spark positions is 8 μm and, thus, an average volume of light collection is ~257 μm^3. At a concentration of 4.08 μM, the number of Ca^{2+}-bound fluo-3 molecules within this volume was calculated to be 6.29×10^5 molecules.

Dividing the calculated number of Ca^{2+}-bound molecules in this volume by their measured mean basal fluorescence signal gave a calibration factor of 2.44 Ca^{2+} ions, bound to fluo-3, per detected photon. The signal mass (sm) of Eq. 3 was converted into moles of Ca^{2+} using the formula:

$$Ca^{2+}\text{-bound fluo-3 (moles)} = 0.41 \times 10^{-23} \cdot \mathrm{sm}(t). \qquad (10)$$

Similarly the flux, f(t) of Eq. 6 is converted to Ca^{2+} current using the formula:

$$I_{Ca(spark)}\ (\text{amps}) = 7.9 \times 10^{-19} \cdot \mathrm{flux}(t). \qquad (11)$$

The average detection threshold for all sparks was a flux equal to $\sim 0.89 \times 10^{-20}$ mol of Ca^{2+} in 10 ms (or ~0.19 pA). The smallest detection threshold, due to variations in the basal fluorescence, was equal to $\sim 0.47 \times 10^{-20}$ mol Ca^{2+} in 10 ms (or ~0.1 pA).

The Fraction of Free Ca^{2+} Detected

To determine whether the fluo-3 was able to track the Ca^{2+} released in a spark, we used two sets of simulations. In each case, finite difference approximations were used to solve a set of partial differential equations for the reaction–diffusion kinetics in a cylindrical coordinate system. The details of this approach are described elsewhere (Kargacin and Fay, 1991; Zou et al., 1999). In the first set of simulations, we examined the result of a 30-ms long period of Ca^{2+} influx (10, 1, or 0.1 pA) from a point source into the cytosol of a cylindrical cell (length = 30 μm and radius = 6 μm) containing 50 mM fluo-3 (i.e., the concentration in the patch pipet). 30 ms was chosen because this was the approximate duration of the longest time to peak for the development of the spark signal mass (see RESULTS). The results of these simulations are shown in Fig. 1 A for 1 pA, and the parameters are provided in the figure legend. As can be seen, fluo-3 binds Ca^{2+} rapidly enough to track the Ca^{2+}. In the absence of endogenous stationary buffer, the fluorescence reports virtually all the Ca^{2+} entering the cytosol; i.e., virtually all the Ca^{2+} (i.e., >90%) is in the bound form. Endogenous mobile buffers should dialyze away through

data as the row above but at a higher gain (×5) to make the fluorescence visible to the eye on the pseudocolor scale used. b plots the measurement of signal mass of the sort exemplified in a for several distances of the epicenter pixel from the plane of focus. n each case, the total fluorescence is computed over a 13.7-μm square region (red boxes) after blurring with the PSF. In each case, the total fluorescence is computed over a 13.7-μm square region (red boxes) after blurring with the PSF. As can be seen, only a small amount of fluorescence is lost even 6 μm out of the plane of focus (dotted line). In general, we estimate that for an average cell, the maximum distance from the plane of focus is 4 μm.

Published November 29, 2000

the patch pipet so they were not included in the simulation. When 230 μM of fixed buffer was included (Robertson et al., 1981; Bond et al., 1984; Kargacin and Fay, 1991), the signal mass was reduced in amplitude, but its onset and peak were unaltered. If the K_d was sufficiently low, the time course of the rising phase was unaffected, but a sag appeared after the cessation of the current. (For each of the stationary buffers used in the simulation, the k_{on} was diffusion limited and the k_{off} was varied to give the K_d's shown [Fig. 1 A, legend]). There is reason to believe that the stationary buffer in these cells has only a small effect in the face of 50 μM fluo-3 (see DISCUSSION).

Similar simulations were carried out with Ca^{2+} currents of 0.1 and 10 pA. Over the range of Ca^{2+} currents from 0.1 to 10 pA, the fluo-3 tracked the total Ca^{2+} in a proportional fashion under each of the buffer conditions. Fig. 1 B shows the total Ca^{2+} bound to fluo-3 at the end of a 30-ms pulse of each of these three values of Ca^{2+} current in the presence and absence of the same fixed buffer shown in Fig. 1 A. Hence, the increase in fluorescence is

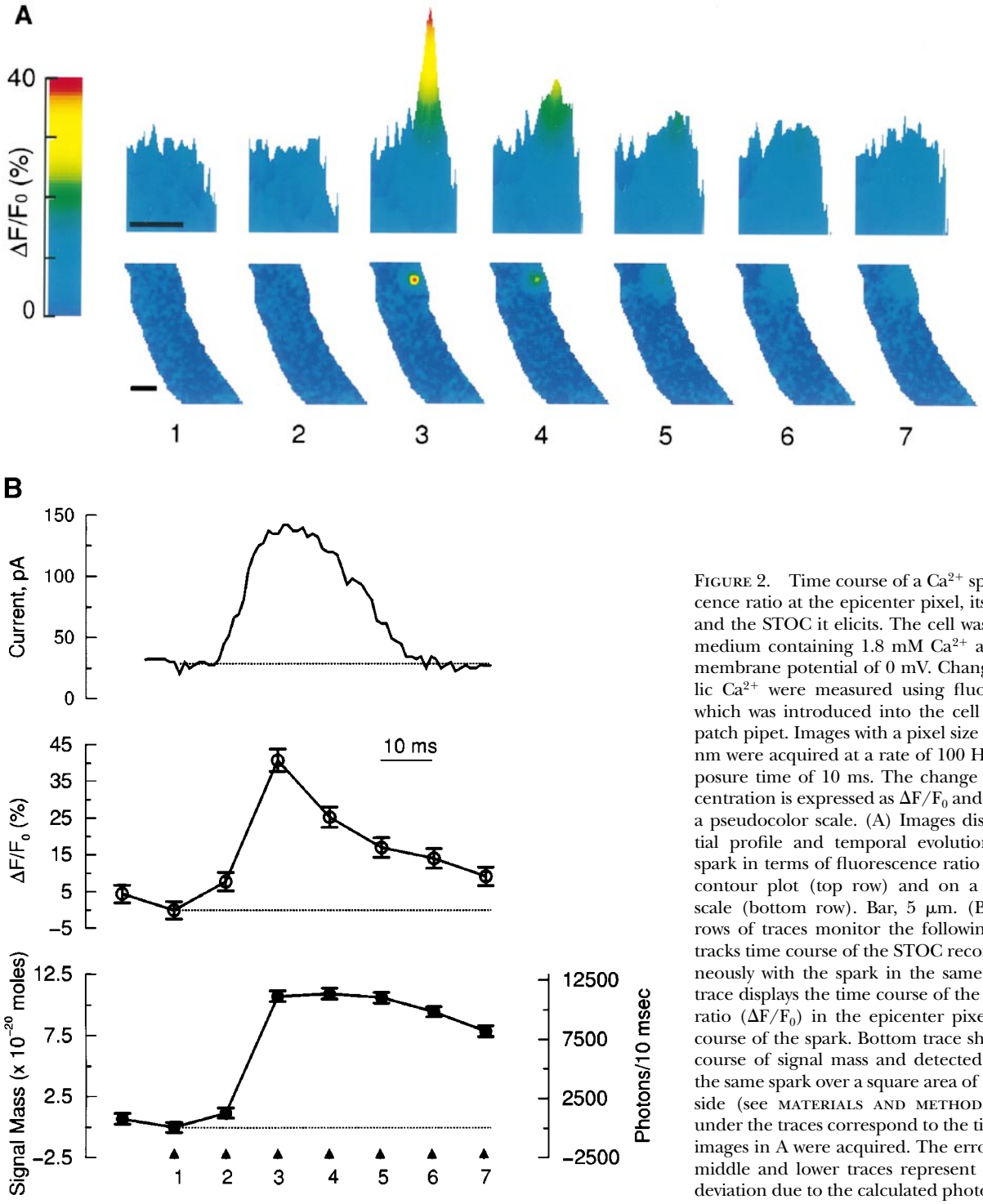

FIGURE 2. Time course of a Ca^{2+} spark's fluorescence ratio at the epicenter pixel, its signal mass, and the STOC it elicits. The cell was bathed in a medium containing 1.8 mM Ca^{2+} and held at a membrane potential of 0 mV. Changes in cytosolic Ca^{2+} were measured using fluo-3 (50 μM), which was introduced into the cell through the patch pipet. Images with a pixel size of 333 × 333 nm were acquired at a rate of 100 Hz with an exposure time of 10 ms. The change in Ca^{2+} concentration is expressed as $\Delta F/F_0$ and displayed on a pseudocolor scale. (A) Images display the spatial profile and temporal evolution of a Ca^{2+} spark in terms of fluorescence ratio ($\Delta F/F_0$) as a contour plot (top row) and on a pseudocolor scale (bottom row). Bar, 5 μm. (B) The three rows of traces monitor the following. Top trace tracks time course of the STOC recorded simultaneously with the spark in the same cell. Middle trace displays the time course of the fluorescence ratio ($\Delta F/F_0$) in the epicenter pixel during the course of the spark. Bottom trace shows the time course of signal mass and detected photons for the same spark over a square area of 13.7 μm on a side (see MATERIALS AND METHODS). Numbers under the traces correspond to the time when the images in A were acquired. The error bars in the middle and lower traces represent the standard deviation due to the calculated photon noise.

Published November 29, 2000

proportional to the quantity of Ca^{2+} released over a range of two orders of magnitude ~1 pA. We expect the Ca^{2+} current to be in the 1-pA range based on previous estimates (ZhuGe et al., 1999; Zou et al., 1999) and on the results obtained here (see RESULTS).

In the first set of simulations just described, the entire cell was used as the collection volume, assuming perfect capture of all the fluorescence throughout the z-axis (i.e., the properties of the imaging system and its point spread function [PSF] were not included in the simulation). A second set of simulations refined the first in two ways: the fluorescence collection area was restricted to a 13.7-μm square area centered on the release site; and an empirically determined PSF was incorporated to examine the effect when the spark was as much as 6 mm removed from the z-plane of focus. (This distance is sufficient for a cell of the thickness used in this study, given that we sought to focus at the cell's center.) The results of the second set of simulations for 1 pA are shown in Fig. 1 C; the simulations were limited to the case where there was no fixed buffer. It is clear that with the 13.7-μm square collection area almost all the fluorescence is captured both for sparks in the focal plane and out of it. (In the worst case, i.e., farthest from the plane of focus, 84% of the fluorescence is monitored.) Finally, it should be noted that, with the widefield system, the time course of the signal mass trace is not affected by the position of the spark release site in the z-axis.

Reagents

All chemicals except fluo-3 (Molecular Probes) were purchased from Sigma-Aldrich.

RESULTS

The Quantity of Ca^{2+} Released into the Cytosol by a Ca^{2+} Spark Can Be Determined Using High Temporal Resolution, Widefield Digital Microscopy

Ca^{2+} sparks and the STOCs elicited by them were simultaneously monitored using a widefield digital imaging system with high sensitivity, low noise, and high temporal resolution in combination with whole-cell patch recording. (See MATERIALS AND METHODS and the results of simulations in Fig. 1.) Fig. 2 illustrates a typical recording of a single Ca^{2+} spark and the STOC it elicits. In Fig. 2 A, a small region of the smooth muscle cell is shown, and a single Ca^{2+} spark is represented on a pseudocolor scale in the bottom row of images and by a contour plot also incorporating the same pseudocolor scale in the top row. (The height of the contour plot provides a measure of relative intensity without introducing subjective color impressions.) In Fig. 2 B, the top trace records the STOC; and the middle trace records the conventional measure of spark amplitude (the fluorescence ratio, $\Delta F/F_0$) for the single pixel (333 × 333 nm) where the fluorescence ratio reaches its highest value (i.e., the epicenter pixel). The bottom trace in Fig. 2 B tracks the signal mass, i.e., the increase in total fluorescence over an area 13.7 μm square (i.e., 41 pixels on a side) and throughout the entire thickness of the cell (~8 μm on average). A collection volume of this size was sufficient both to prevent loss of fluorescence because of diffusion of Ca^{2+} and bound fluo-3 away from the point of release and to capture 84% or more of the fluorescence from sparks originating outside the plane of focus (Fig. 1). Hence, the signal mass is proportional to the total quantity of cytosolic Ca^{2+} accumulated over time, i.e., the integral of net Ca^{2+} current into the cytosol. Here, as elsewhere, the signal mass is given in terms of moles of Ca^{2+} using the calibration described in MATERIALS AND METHODS. This calibration assumes that there are no significant buffers other than fluo-3 acting over this time frame so that the value for the quantity of Ca^{2+} constitutes a lower bound (see DISCUSSION). It is important to note that the signal mass is not a measure of Ca^{2+} concentration. The slope of the signal mass trace is proportional to the net Ca^{2+} current into the cytosol from the SR through the RyRs or, in terms of charge, the net Ca^{2+} current into the cytosol. We refer to this as the spark Ca^{2+} current or $I_{Ca(spark)}$; as with the signal mass, the value given for $I_{Ca(spark)}$ is a minimum. The spark current is a useful measure since it provides a way of examining the Ca^{2+} current of the RyRs in the cell under physiological conditions as opposed to recordings in an artificial bilayer system.

The record of signal mass, unlike that of $\Delta F/F_0$ at the spark epicenter pixel, does not return to baseline, but rather remains at a plateau level for the period shown. The half-time for decay of the fluorescence ratio was ~15 ms in this example, whereas the half-time for the decline of the signal mass was well in excess of 100 ms. For the entire population of sparks analyzed, the average half-time of decay for the fluorescence ratio was 16 ± 0.4 ms, whereas the signal mass had not decayed to half its peak value even after 100 ms. Hence, it appears that diffusion into the surrounding cytosol accounts for most of the decline in Ca^{2+} at the spark epicenter. This result is consistent with estimates for Ca^{2+} sparks in cardiac cells where diffusion accounts for ~80% of the decay in spark amplitude (Gomez et al., 1996). Moreover, the existence of the plateau phase indicates that the volume subtended by the area over which the fluorescence is monitored is sufficiently large to capture virtually all the fluorescence due to bound Ca^{2+}. If the monitored area was not large enough, then there would be a decay as the Ca^{2+} and bound fluo-3 diffused away. Finally, the rising phase of signal mass lasted 20 ms or less in most cases and exceeded 30 ms only in a few instances.

The signal mass measure, when implemented with widefield microscopy, is affected minimally by the z-axis location of the spark in cells of the thickness used here, given the area of the x-y plane from which fluorescence is collected and the PSF of the widefield digital system (see Fig. 1 C and MATERIALS AND METHODS). That is, virtually the entirety of the fluorescence is captured by this system whether or not the spark is in focus. Moreover, since the system captures sparks over the entire

Published November 29, 2000

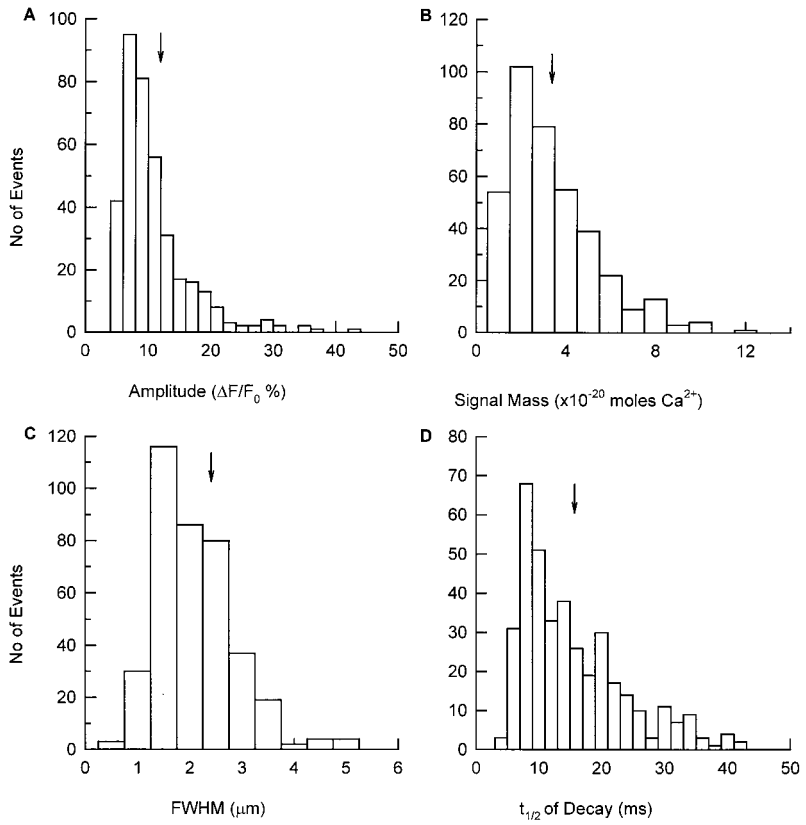

FIGURE 3. Histograms of Ca^{2+} spark amplitude, signal mass, full width at half maximum (FWHM), and $t_{1/2}$ of decay. 365 Ca^{2+} sparks from 31 cells that were identified based on criteria described in the MATERIALS AND METHODS are used to construct the plots. Arrows indicate the mean of the distribution for each parameter. Values of mean ± SEM are as follows: 11.6 ± 0.29% for Ca^{2+} spark amplitude; 3.4 ± 0.1 × 10^{-20} mol Ca^{2+} for signal mass; 2.4 ± 0.04 μm for FWHM; and 16 ± 0.45 ms for $t_{1/2}$ of decay. Except for the signal mass, all measurements are based on $\Delta F/F_0$ at the epicenter pixel.

x-y plane lying within the field, no distortion is introduced in this plane for either the signal mass measure or for the fluorescence ratio. In sum, the widefield system is ideally suited for the signal mass approach. A widefield system is also suited for the study of sparks in a cell like smooth muscle and neurons where the location of the sparks is not known a priori as it is in striated cells with their well demarcated t-tubular system.

The error bars in the middle and bottom traces of Fig. 2 B represent the SD due to the calculated photon noise. Two points deserve mention. First, our initial criterion for identifying an event as a Ca^{2+} spark is an increase of 5% in the fluorescence ratio $\Delta F/F_0$ (lasting two or more frames), which is a level equal to 1 SD above the noise (Fig. 2 B, middle trace). Second, the signal to noise ratio, which is approximately equal to the square root of the total fluorescence, is higher in the signal mass record than in the record of fluorescence ratio since more photons are collected in the former. The low noise in the signal mass is also due to the high signal to noise ratio of the digital imaging system and CCD camera.

Characterization of Ca^{2+} Sparks

Although sparks have been studied previously in a number of smooth muscle types (Nelson et al., 1995; Mironneau et al., 1996; Bolton and Gordienko, 1998; ZhuGe et al., 1998, 1999; Pabelick et al., 1999; Collier et al., 2000), distributions of parameters characterizing the sparks have not been reported. We examined the properties of a population of 365 sparks in 31 smooth muscle cells (Fig. 3). The percent change in fluorescence (Fig. 3 A) displayed a distribution with a single peak at 11.6% and an extended tail, giving a range of one order of magnitude. The distribution of the signal mass for each spark is given in Fig. 3 B. It has a single peak, an extended tail, and a total range of >13-fold, thus, resembling the distribution in Fig. 3 A. Both distributions are consistent with a continuum rather than with several discrete populations in a hierarchy, and resemble Ca^{2+} puffs in this respect (Sun et al., 1998; Thomas et al., 1998). It is also noteworthy that the range in the distribution for the signal mass is somewhat greater than that for fluorescence ratio. Since the signal mass is essentially independent of focus, the observed spark variability in this is real and not simply a result of variation with respect to location of the spark site in the z-plane. Also shown are the distributions of full-width at half maximum amplitude (Fig. 3 C) and the half-time of decay (Fig. 3 D), both based on the fluorescence ratio ($\Delta F/F_0$).

Signal Averaging Based on STOCs Makes Possible a Kinetic Analysis of Ca^{2+} Signal Mass

To analyze the relationship between the underlying $I_{Ca(spark)}$ through the RyRs during a spark and the corresponding STOCs, we wished to examine the kinetics of each. To do so, we carried out the signal averaging pro-

Published November 29, 2000

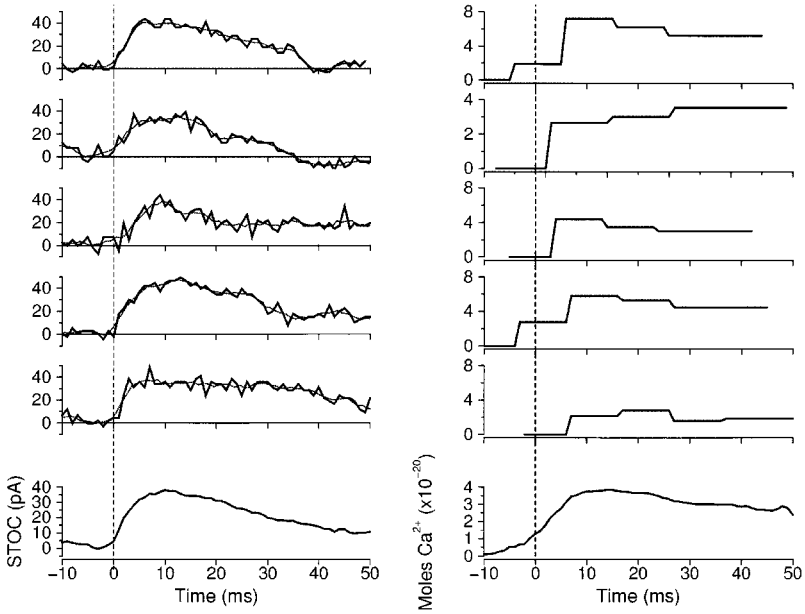

FIGURE 4. Alignment and averaging of Ca^{2+} spark signal mass by using the corresponding STOCs. Five examples of STOC recordings (1-kHz sampling rate; solid lines) and their three-point running averages (smoothed traces marked by dotted lines) are shown on the left. STOCs are aligned at time 0 (vertical dashed line), which is the point when the smoothed trace reaches 5-pA level above baseline. STOCs are averaged over time with respect to the zero time point to generate a mean STOC (bottom left). Five signal mass traces (0.1-kHz sampling rate) in correspondence to each STOCs are displayed on the right. Time 0 for each signal mass measurement is taken from its corresponding STOC and marked by another vertical dotted line. The signal mass traces are then averaged with respect to this zero point, yielding the mean trace (bottom right).

cedure illustrated in Fig. 4. The procedure is illustrated in Fig. 4 for five different STOCs (left) and the signal mass of the corresponding sparks (right). First, the STOCs are all aligned at time 0 when their three-point smoothed signal reached the 5-pA level above baseline, as determined from custom-made software. Time 0 is taken as the initiation point for the STOC, and the group of STOCs is averaged over time with respect to this initiation point (Fig. 4, bottom left). For each corresponding record of signal mass, the same time point is assigned as the zero time (Fig. 4, right). The signal mass traces are averaged with respect to this zero point, yielding the mean trace (Fig. 4, bottom right). The zero time for the averaged signal mass is the initiation time for the STOC not the spark. As would be expected, the signal mass begins to rise before the initiation point for the STOC and, hence, the onset of the increase in signal mass corresponds to a negative time along the x-axis.

Ca^{2+} Sparks Are Caused by the Concerted Opening of Multiple Ryanodine Receptors

Do sparks with Ca^{2+} signal mass of varying amplitudes have different underlying Ca^{2+} currents? If the larger signal mass is due simply to a single RyR opening for a longer time, then the underlying $I_{Ca(spark)}$ will be the same; if the sparks are due to the concerted opening of multiple RyRs, $I_{Ca(spark)}$ will vary. To examine this question, we grouped the sparks into quarters based on the magnitude of the signal mass for each spark. Then, we used the signal averaging technique outlined in Fig. 4. The results are shown in Fig. 5, with the signal mass shown in A and B, the latter on an expanded scale; the corresponding STOC traces are shown below in C and D. The slopes of the plots in Fig. 5 B, which are proportional to the mean $I_{Ca(spark)}$ for each of the groups, differ by more than fivefold. Thus, not all sparks have underlying Ca^{2+} currents of the same amplitude; rather the sparks of larger signal mass are generated by a larger mean $I_{Ca(spark)}$. The data in Fig. 5 B are useful since they provide an estimate of the range of values for $I_{Ca(spark)}$ over the population of sparks. The slopes in Fig. 5 B are 0.08, 0.23, 0.23, and 0.45×10^{-20} mol Ca^{2+}/ms, which correspond, respectively, to 0.15, 0.44, 0.44, and 0.87 pA of Ca^{2+} current. Assuming that each RyR acts as a single pore, the more than fivefold range in these values indicates that a substantial fraction of the sparks are due to the opening of multiple RyRs. The values for $I_{Ca(spark)}$ calculated in Fig. 5 B provide a minimum estimate since buffers other than fluo-3 and the action of ion pumps and exchangers, if they have a substantial effect, will decrease the measured signal mass. At the acquisition rate used, our measurements disclose no clear evidence for anything other than a constant slope on the rising phase of the signal mass, i.e., a constant $I_{Ca(spark)}$ (but see DISCUSSION). The simplest conclusion is that the Ca^{2+} current approximates a step function. Assuming that the underlying Ca^{2+} currents are step functions at least over the first 10 ms of the spark, low pass filtering because of the image acquisition rate leads to an underestimate of the current by about one third. Correcting for such filtering leads to values of mean $I_{Ca(spark)}$ equal to 0.23, 0.66, 0.66, and 1.31 pA. For comparison, Mejia-Alvarez et al. (1999) have recently estimated that the Ca^{2+} current through a single cardiac RyR in a bilayer is 0.35 pA. We consider in greater detail in the DISCUSSION how the values found in this study compare to single RyR Ca^{2+} currents measured in bilayers and to sparks in other sys-

Published November 29, 2000

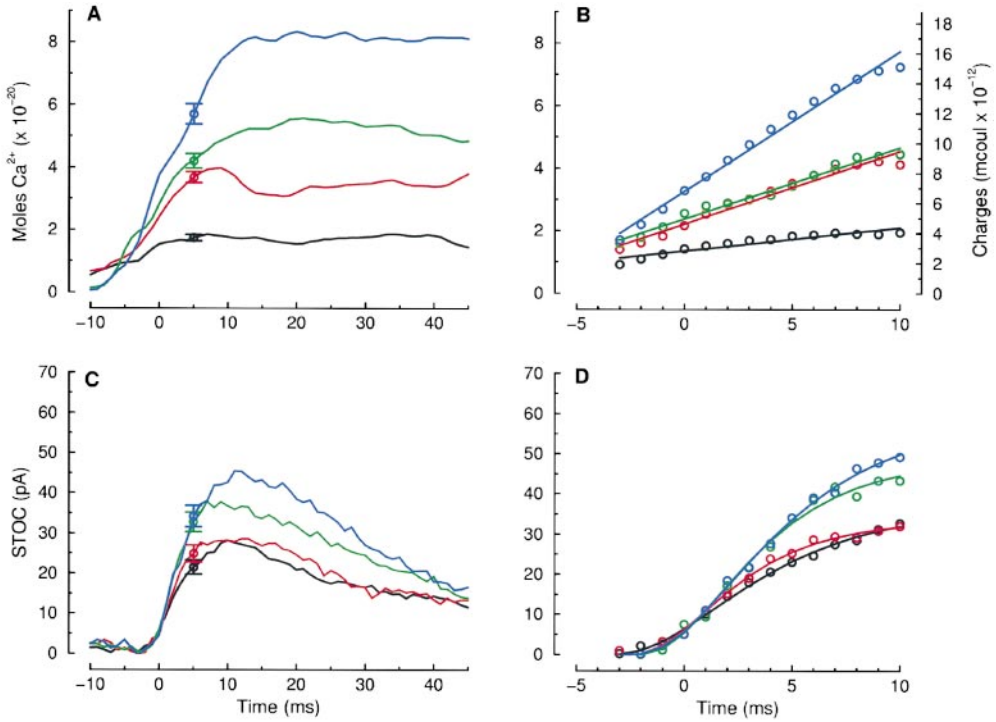

FIGURE 5. Mean $I_{Ca(spark)}$ varies more than fivefold. (A) The averaged record for each of four groups of sparks arranged from smallest to largest. 146 individual sparks were ranked based on peak amplitude of their signal mass, and then divided into quarters, from smallest to largest. Sparks within each group were aligned and averaged according to the approach illustrated for a smaller number of events in Fig. 4 (i.e., the temporal alignment within each group is based on the corresponding STOCs). (B) Determination of the mean $I_{Ca(spark)}$ from the slope of the initial rise of the signal mass traces in A. On the right vertical axis, the signal mass is converted to total charge. The slopes (i.e., mean $I_{Ca(spark)}$) were 0.15, 0.44, 0.44, and 0.87 pA for the four groups from smallest to largest. (C) The averaged STOC traces for the four groups corresponding to the sparks in A. Individual STOCs were sorted based on their corresponding spark signal mass amplitude, aligned, and averaged as described in Fig. 4. Open circles in both A and B mark the 5-ms time point discussed in the text. (D) Expanded time scale of the rising phase of the four groups of STOCs. Circles are the data points for the activation phase of STOCs on an expanded time scale. Solid lines are the least square fits to the data from time 0 to 10 ms using the following expression: $I(t) = I_{max}(1 - \exp[-(t + t_{del})/\tau])^3$, where I_{max} is the peak current, t_{del} is the time for current to rise 5 pA above baseline (STOCs <10 ms in rising phase were omitted for the fitting). These fits yielded time constants (τ) of 4.4, 3.1, 3.5, and 4.3 ms for each of the four groups, from smallest to largest.

tems. It is clear that certain features of the data in Fig. 5 speak to the relationship between a Ca^{2+} spark and the STOC that it generates. This will be considered in more detail in the next section.

STOC Amplitudes in the Presence and Absence of 50 μM Fluo-3

A comparison was made between the STOCs recorded in the presence and absence of fluo-3 (50 μM) in the patch pipet. The results are shown in Fig. 6. There was no apparent difference in the two populations ($P = 0.244$, *t* test). Hence, fluo-3 at this concentration does not change the $[Ca^{2+}]$ at the interior surface of the BK channels enough to affect their activation.

Fluorescence Ratio Estimate of Ca^{2+} Concentration during a Spark Is a Poor Predictor of STOC Amplitude

Is the relative $[Ca^{2+}]$ at the peak of a spark, as estimated by $\Delta F/F_0$ at the epicenter pixel, a good predictor of the corresponding STOC? Fig. 7 A shows a plot relating these two parameters for 255 sparks. Those sparks that did not generate STOCs are assigned a value of 0 and plotted on the abscissa. Although the correlation between $\Delta F/F_0$ and STOC amplitude is significant, it is evident from the plot that the correlation is quite weak ($r = 0.163$ and $P = 0.026$; Spearman rank order coefficient). (In calculating the correlation coefficient [r], the STOC-less sparks appearing on the abscissa are omitted; including these points would further weaken the correlation.) The FWHM, as determined from the fluorescence ratio (Fig. 7 B) is also weakly correlated with STOC amplitude ($r = 0.158$ and $P = 0.031$). These relatively poor correlations might result from the fact that the percent change in fluorescence is affected by the plane of focus (z-axis) in which the spark occurs. Hence, we examined the correlation for those sparks that appeared at the lateral edges of the cell in two-dimensional images. Since we attempted to focus on the center of the cell, these sparks were more likely to lie in the plane of microscope focus. But for this data set, the correlation between STOCs and either parameter did not grow stronger (not shown). Another possible way to correct for this problem is to use the signal mass as a measure of spark intensity since it is almost completely insensitive to the z-plane in which the spark occurs. Using the signal mass, the correlation im-

Published November 29, 2000

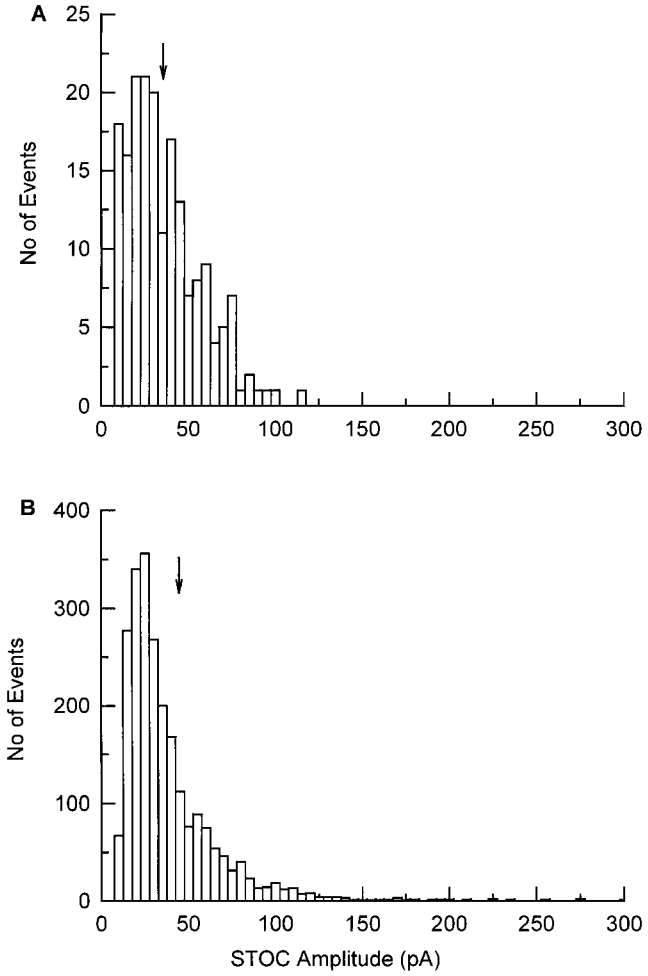

FIGURE 6. 50 μM fluo-3 in the cytosol does not change the mean amplitude of STOCs. STOCs were acquired using whole-cell recording at a holding potential of 0 mV. Values of STOCs were 38.4 ± 1.5 pA in the presence of 50 μM fluo-3 in the patch pipet (A, total number of events = 180) and 40.8 ± 0.6 pA in the absence of fluo-3 (B, total number of events = 2,348 from 15 cells). Evaluations of means with an unpaired *t* test yielded a significance value of 0.244. Arrows indicate the mean of the distribution in two conditions.

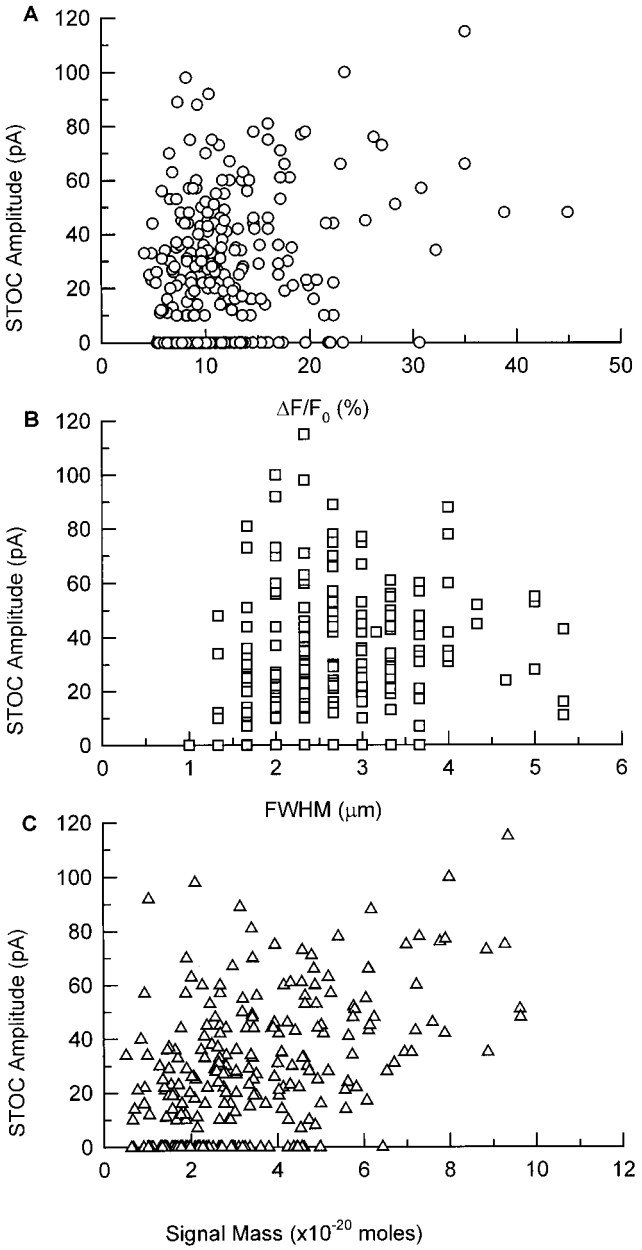

FIGURE 7. Correlations of Ca^{2+} spark parameters with STOC amplitude. Displayed are the plots of amplitude of STOC against spark amplitude (A), FWHM (B), and signal mass (C). Rank order correlation analysis yielded Spearman correlation coefficients (r) and significance levels (*P*) as follows: r = 0.163 and *P* = 0.026 for STOC amplitude versus spark amplitude; r = 0.158 and *P* = 0.031 for STOC amplitude versus FWHM (based on $\Delta F/F_0$); and r = 0.40 and *P* = 0.001 for STOC amplitude versus signal mass. Sparks that failed to cause STOCs are plotted on the abscissa.

proves somewhat (Fig. 7 C), but it remains weak and is a poor predictor of spark amplitude (r = 0.40 and *P* = 0.001; Spearman rank order coefficient).

Many Ca^{2+} Sparks Fail to Cause STOCs

Although most Ca^{2+} sparks triggered STOCs, 21% did not and these are plotted on the abscissa in Fig. 7. Two such STOC-less sparks are illustrated in Fig. 8; the spark shown in Fig. 8 A lies at the edge of the cell. Among sparks that clearly lay at the cell's edge, 23% failed to elicit STOCs. Thus, the failure to cause STOCs cannot simply be attributed to spark generation at a site far from the membrane. (The same conclusion about STOC-less sparks emerged from an earlier study on a different smooth muscle preparation. In that case, 3-D imaging was used to locate the sparks unambiguously, and the STOC-less sparks were somewhat closer to the membrane than the average [Kirber et al., 1998].) We asked whether the sparks that triggered STOCs (a total of 290) differed from those that did not (a total of 75). The following significant differences were found

Published November 29, 2000

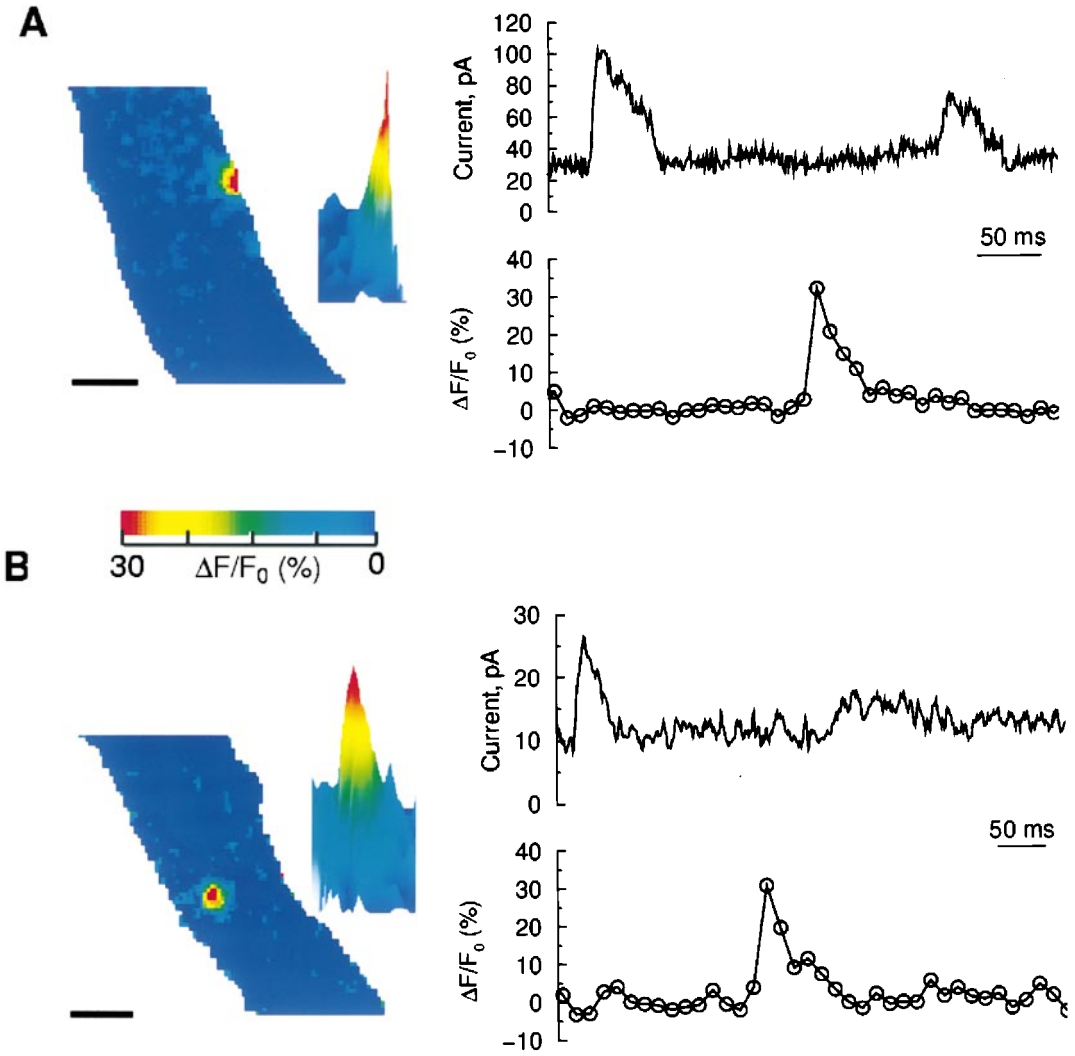

FIGURE 8. Ca^{2+} sparks that fail to induce STOCs. Images on the left were acquired at the peak of two sparks. The membrane currents and time courses of $\Delta F/F_0$ at the epicenter pixel for these sparks are displayed on the right. (A) A spark occurs close to the cell surface; note the flattened surface of the contour plot at the cell's edge. (B) Spark position is ambiguous; it could lie at the cell's top or bottom surface or in the interior. (The sparks for the remaining STOCs are not apparent in this figure because the $\Delta F/F_0$ traces only plot the epicenter pixel of the displayed sparks and the images display only the max $\Delta F/F_0$ time point of the spark whose time course is plotted on the right.)

(mean ± SEM) for sparks with STOCs and sparks without STOCs, respectively: $\Delta F/F_0$ (in percent), 12.6 ± 0.5 vs. 10.5 ± 0.5, $P = 0.004$; FWHM, 2.7 ± 0.1 μm vs. 2.2 ± 0.1 μm, $P = 0.001$; signal mass, 6.2 ± 0.3 × 10^{-20} mol Ca^{2+} vs. 4.0 ± 0.2 × 10^{-20} mol Ca^{2+}, $P = 0.001$; and $t_{1/2}$ of decay, 16.0 ± 0.5 vs. 15.4 ± 0.91, $P = 0.269$. Even though the two spark populations are significantly different by these measures, the overlap in their distributions is substantial as can be seen in Fig. 7, where the STOC-less sparks appear on the x-axis. Thus, relatively small sparks may generate STOCs, and relatively large ones may fail to do so. This suggested to us that the coupling between RyRs and BK channels might be variable, with the STOC-less sparks lying at one extreme.

Variation in Signal Mass–STOC Coupling Ratio Is due in part to Variation in Ratio of RyRs/BK Channels

Are larger STOCs caused by $I_{Ca(spark)}$ of greater amplitude? To address this question, we divided the population of STOCs into quarters, grouped from smallest to largest so that the smallest STOCs all fell into the first quarter and the largest into the fourth quarter. This was done to maximize the observable differences in $I_{Ca(spark)}$ underlying STOCs of different amplitudes. The same signal averaging procedure, as shown in Fig. 4, was carried out for each quarter of the STOC population. The averaged STOCs for each quarter are shown in Fig. 9 A, and the time course of the corresponding mean signal mass in Fig. 9 B. The temporal alignment

Published November 29, 2000

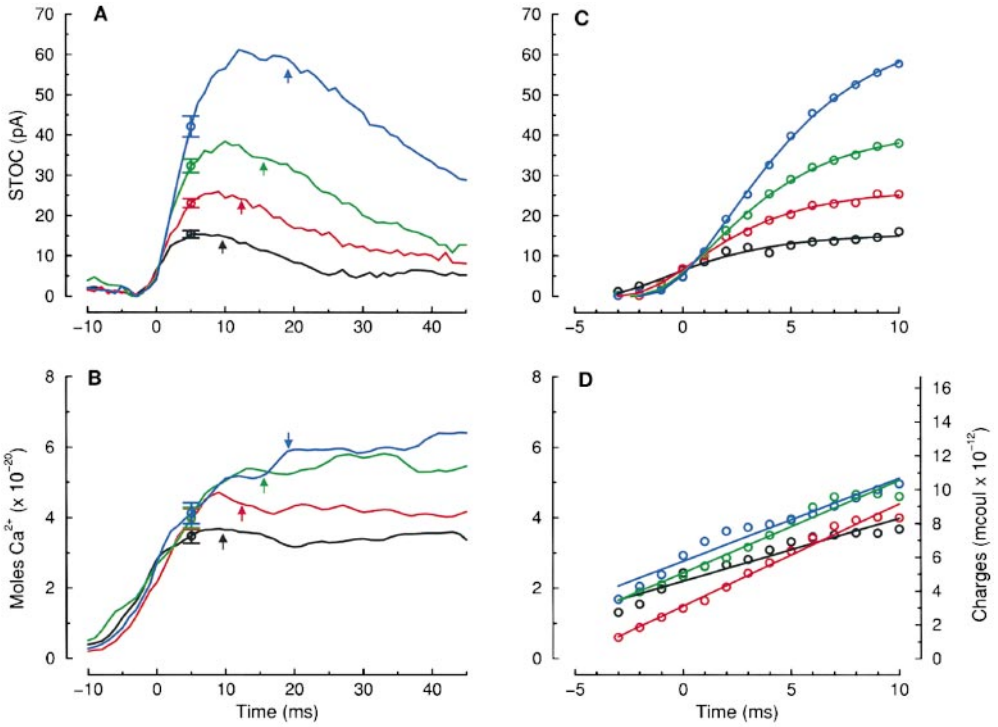

FIGURE 9. Large differences in mean STOC amplitude accompany small differences in mean signal mass and $I_{Ca(spark)}$. (A) The averaged record for each of four groups of STOCs arranged in order from smallest to largest. 146 individual STOCs were ranked based on their peak amplitude and divided into quarters from smallest to largest. STOCs within each group were aligned and averaged according to the approach illustrated for a smaller number of events in Fig. 4. Thus, the grouping into quarters in this instance is based on the STOC, in contrast to Fig. 5; but the temporal alignment within each group is based on the STOCs, which is similar to Fig. 5. The arrows denote the onset of STOC decay. (B) The signal mass traces for the four groups of sparks corresponding to the STOCs in A. Individual Ca^{2+} sparks were sorted based on their corresponding STOC amplitude and aligned and averaged as described in Fig. 4. Open circles in both A and B mark the 5-ms time point discussed in the text. At this point there is approximately a three-fold difference in mean STOC amplitude but a very small difference in signal mass. (Arrows again denote the onset of STOC decay as determined from the traces in A above; they are included on the signal mass traces to facilitate comparison.) (C) The rising phase of the four groups of STOCs. Circles are the data points for the activation phase of STOCs on an expanded time scale. The activation phase for the four groups of STOCs were fit according to the same equations given in the legend to Fig. 5 D. These fits yielded time constants (t) of 3.2, 3.2, 3.4, and 4.00 ms for each of the four groups, from smallest to largest. (D) Determination of the mean $I_{Ca(spark)}$ from the slope of the initial rise of the signal mass traces in B. On the vertical axis, the signal mass is converted to total charge. The slopes (i.e., mean $I_{Ca(spark)}$) were 0.38, 0.60, 0.54, and 0.50 pA for the four groups, from smallest to largest.

of the signal mass traces here is determined by the STOCs, as described above for Fig. 4.

The peak STOC amplitude for the four groups varies by a factor of four (Fig. 9 A), whereas the corresponding signal mass peak varies only by a factor of two (Fig. 9 B). Although the mean time to peak (TTP) for the larger STOCs and the corresponding signal mass (Fig. 9, A and B) tend to be longer, the longer duration cannot fully account for larger STOC amplitude. This becomes apparent on examination of the 5-ms time point designated by open circles on the traces. At this point, it can be seen that the signal mass for the four groups varies by only a small amount (Fig. 9 B, circles) whereas the STOC amplitude varies by almost a factor of three (Fig. 9 A, circles). At this time point the mean signal mass for the smallest group of sparks (black line) reaches its peak and the others continue to rise. Hence, at this point, approximately the same mean signal mass and the same mean $I_{Ca(spark)}$ gives rise to a STOC current that varies by about threefold for the four groups. The mean $I_{Ca(spark)}$ for each of the four groups was calculated explicitly from the slope of a straight line fitted to the data points beginning at the onset of the rise in signal mass and ending at the time that the signal mass reaches its peak (Fig. 9 D). As can be seen, the mean $I_{Ca(spark)}$ varies by only a small amount for the four groups, with the largest difference lying between the smallest quarter and the others. Moreover, the rank order of the mean $I_{Ca(spark)}$ for the same four groups is not the same as that of the STOC amplitude at the 5-ms time point.

We term the ratio of signal mass to STOC current the "coupling ratio." The large variation in coupling ratio at the 5-ms time point indicated by the circles in Fig. 9 could be explained in two fundamental ways. The first is that the number of BK channels (N) per RyR is variable. The second is that the number of BK channels (per RyR) does not vary, but the probability of their being in the open state (P_o) does. In turn, this variability in P_o may occur for two reasons. First, the BK channels at different spark sites may have different kinetic properties. For example, because of the presence of different BK channel isoforms; or second, the BK channels may lie at different distances from the RyRs at different spark sites. Consider the possibility that P_o varies be-

Published November 29, 2000

cause of variation in the kinetic properties of the BK channels. In this case, a larger fraction of a constant number of BK channels (per RyR) would be activated in the same period of time because of faster kinetics. The kinetics of the rising phase of the four groups of STOCs are analyzed in Fig. 9 C; for each group, the data points (open circles) were fitted by the equations and parameters given in the figure legend (solid lines). We chose these expressions because they were previously used by Markwardt and Isenberg (1992) to fit the responses of smooth muscle BK channels in excised inside-out patches to rapid jumps in $[Ca^{2+}]$ (see DISCUSSION). The kinetics of the rising phase for the four groups does not vary systematically from smallest to largest; and there is little difference among the three smallest groups. Moreover, the rate of rise for the largest group of STOCs is slowest and that for the smallest group is fastest. This is the opposite of the expected order if differences in BK channel kinetics were to underlie the differences in STOC amplitudes caused by the same Ca^{2+} current.

Consider next the possibility that P_o varies because of variability in the distance between the RyRs and BK channels at different spark sites. In this case, the smaller STOCs should result from a greater distance between BK channels and RyRs; such smaller STOCs should arise from the exposure of BK channels to lower $[Ca^{2+}]_i$ and, hence, the P_o should be lower and the kinetics slower. Here again, the fact that the smallest group of STOCs has the fastest kinetics, and the largest group the slowest kinetics, argues against this alternative. We conclude that P_o for the BK channels is not different at the different spark sites. Rather, the first of the alternatives is correct, i.e., the number of BK channels per RyR is not constant but variable.

These results also place a restriction on the role of Ca^{2+} diffusion as a factor in the variability in coupling ratio. Since the mean $I_{Ca(spark)}$ is the same at the 5-ms point for the four groups, the spatial profile of $[Ca^{2+}]$ would appear to be the same at that point in time. This rules out recruitment of BK channels due to diffusional spread of Ca^{2+} as the cause of the difference in coupling ratios, at least up to this time point.

Another factor apparently contributes to the larger STOCs at points later than the 10-ms time point as marked in Fig. 9 A. As noted above, the TTP is longer for the larger STOCs, 8.6 ± 0.7, 11.0 ± 0.8, 12.0 ± 0.9, and 13.9 ± 0.9 ms for the four groups ($P < 0.001$ by analysis of variance). This is apparently due to the fact that the Ca^{2+} current duration is greater for the longer STOCs. Since the STOCs should begin to decay when the Ca^{2+} current turns off, the larger STOCs should also have later times for the onset of their decay. In fact, this is the case with the mean lapse in time from the onset of the STOC to the onset of decay for the four groups being 9.6 ± 0.9, 12.4 ± 1.0, 15.6 ± 1.2, and 19.1 ± 1.6 ms ($P < 0.001$ by analysis of variance). These time points are indicated by the arrowheads in the STOC traces of Fig. 9 A; the arrowheads in Fig. 9 B mark the corresponding points on the signal mass traces.

STOC Activation Kinetics Are Not Altered by Variations in Mean $I_{Ca(spark)}$

The qualitative relationship between sparks and STOCs agrees with the conclusions that emerge from an examination of Fig. 5; i.e., the mean Ca^{2+} signal mass at its peak varied by more than fivefold, whereas the mean peak STOC amplitude varied by less than a factor of two. At the 5-ms time point (Fig. 5, A and C, circles), this discrepancy is also evident, with an approximate threefold difference in signal mass among the groups but a 1.67-fold difference in STOC amplitude. Again, since this comparison is made for the same point in time, differences in the time to peak of the spark signal mass (i.e., differences in duration of $I_{Ca(spark)}$) cannot account for the difference in coupling ratio at this time point. Moreover, large variations in $I_{Ca(spark)}$ and Ca^{2+} signal mass of the spark did not alter the BK channel kinetics during the rising phase of the STOC. Since the differences in mean signal mass (Fig. 5 A) and $I_{Ca(spark)}$ (Fig. 5 B) were substantial among the four groups of data, it was possible to examine the effect of signal mass and $I_{Ca(spark)}$ on the rising phase of the STOCs (Fig. 5 D). Here, the kinetics of the rising phase did not vary systematically among the groups (from smallest to largest) despite a fivefold difference in the mean $I_{Ca(spark)}$

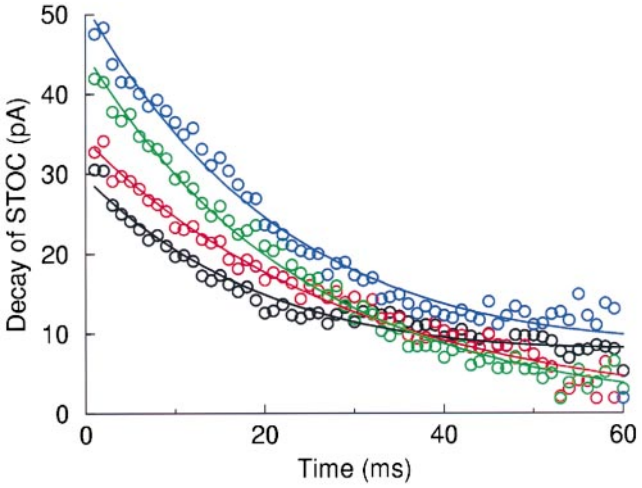

FIGURE 10. The rate of decay of the STOC is independent of signal mass and $I_{Ca(spark)}$. The decay kinetics of averaged STOCs that were sorted according to their corresponding signal mass amplitude as in Fig. 5. The plot shows the decay for each of the four groups of STOCs shown in Fig. 5 C. The circles are the data points; the solid lines represent a single exponential fit to the decay for each group beginning 5 ms after the onset of decay and ending with the value at 60 ms. The time constants for the fit are 25, 24, 30, and 24 ms for the four groups, from smallest to largest.

Published November 29, 2000

(Fig. 5 B) over the first 10 ms. Finally, Ca^{2+} currents that are considerably larger than the ones in Fig. 9 D can be monitored by this system, as is evident from Fig. 5 B, confirming the simulations illustrated in Fig. 1.

The Decay Rate of STOCs Corresponds to the BK Channel Open Time and Is Independent of the Magnitude of the Signal Mass and $I_{Ca(spark)}$

Does the rate of decay of the STOC depend on the magnitude of the spark signal mass or the underlying $I_{Ca(spark)}$? To address this question, the rate of STOC decay was studied by using the grouping in Fig. 5. The results are shown in Fig. 10 where the data points (circles) during the decay for each group of STOCs was fit by a single exponential with the time constants given in the figure legend. As was shown in Fig. 5, both the mean $I_{Ca(spark)}$ and mean signal mass vary more than fivefold among the four groups. Nevertheless, as is evident from Fig. 10, the rate of STOC decay is indistinguishable among three of the four groups, and the time constants do not vary in a systematic fashion from small to large among the groups. These time constants are close to values for the mean open time of BK channels in the same cells in the presence of 1 or 10 μM Ca^{2+}, which were 20–40 ms (Singer and Walsh, 1987) and quite insensitive to $[Ca^{2+}]$. Moreover, the time constants are roughly the same as Markwardt and Isenberg (1992) found for BK channels in inside-out patches at the end of a rapid step change in $[Ca^{2+}]$ at 0 mV in a different smooth muscle preparation. In that study, the decay was well fit by a single exponential with a time constant at 0 mV, which, on average, was 37 ms and was not sensitive to the preceding $[Ca^{2+}]$. These findings are consistent with a drop in $[Ca^{2+}]$ at the BK channels to subactivating levels upon the termination of $I_{Ca(spark)}$, a drop which is rapid in comparison to the slower deactivation kinetics of the BK channels. Finally, the agreement of the decay time constant with the mean open time of BK channels in this preparation is another piece of evidence that BK channels are responsible for STOCs.

Simulations of Changes in $[Ca^{2+}]$ in the Spark Microdomain Based on Measured $I_{Ca(spark)}$

How rapidly is the steady state $[Ca^{2+}]$ profile established in the vicinity of the Ca^{2+} release site? How elevated is the concentration? How rapidly is it dissipated? And how fast is this establishment and dissipation in comparison to the STOC kinetics? To answer these questions, we simulated the consequences of a 15-ms pulse of Ca^{2+} current flowing into the cytosol. This approximates the average time for the signal mass to reach its peak, i.e., the time from onset to termination of the $I_{Ca(spark)}$. Based on the measurements given in Fig. 5, we used values of 0.2 and 1 pA for the Ca^{2+} current in the absence of fixed buffer, and 0.9 and 4.5 pA in the presence of 230 μM fixed buffer with the highest Ca^{2+} affinity (Fig. 1). (These represent the two extremes of possible conditions, i.e., the condition where fixed buffer is negligible and where the fixed buffer is of the highest likely concentration and affinity for Ca^{2+}.) We used a step function for $I_{Ca(spark)}$ since the rate of rise of the signal mass was well fit by a straight line. The results are shown in Fig. 11 A. (The heavy black line in each panel indicates the isoconcentration line for 2 μM Ca^{2+}, the approximate EC_{50} for BK channels in this preparation at 0 mV [Singer and Walsh, 1987].) In each case, the steady state concentration at a radial distance of 200 nm or less reaches its near-final level within 1–2 ms of the onset of $I_{Ca(spark)}$. This is faster than the rise time of the STOCs (Fig. 5 and 9). After the first 1–2 ms at radial distances of 200 nm or less, there is little or no increase in $[Ca^{2+}]$. Subsequent small increases in $[Ca^{2+}]$ at this distance are most evident in the presence of fixed buffer at higher current levels (Fig. 11 A, c and d). But in this case, the concentrations are sufficiently high that a $[Ca^{2+}]$ of 10 μM or more is achieved within 1–2 ms. Thus, within 200 nm, a $[Ca^{2+}]$ is quickly established that is either constant or well in excess of the EC_{50}.

This can be more readily appreciated in Fig. 11 B, where $[Ca^{2+}]$ is plotted as a function of time at a constant distance of 200 nm. The dashed lines indicate the $[Ca^{2+}]_{EC50}$ of the BK channels for Ca^{2+}. Either the $[Ca^{2+}]$ rises quickly to a near constant level or it creeps up more slowly, but only after exceeding the EC_{50} within 1–2 ms. In either event, the BK channels will respond as though the $[Ca^{2+}]$ is unchanging after the first 1–2 ms. Thus, a step of Ca^{2+} current (i.e., $I_{Ca(spark)}$) produces, within a microdomain of 200 nm or less in radius, a condition similar to applying a rapid step change in $[Ca^{2+}]$ to BK channels in an excised inside-out patch, as Markwardt and Isenberg did (1992). Finally, if the BK channels lie close enough to the release site (e.g., within 100 nm), then for all levels of Ca^{2+} current, the BK channels will be exposed to $[Ca^{2+}]$ well in excess of the EC_{50} within 1–2 ms. This could account for the similarity of the kinetics of the rising phase of the STOCs at all levels of $I_{Ca(spark)}$ (Fig. 5).

Examination of the $[Ca^{2+}]$ profile at the end of the $I_{Ca(spark)}$ pulse shows a continuing presence of high levels of Ca^{2+} in the presence of the high affinity fixed buffer (Fig. 11 A, c and d). We used the concentration and affinity of the fixed buffer shown to represent a possible extreme effect on the STOC. However, it appears that the effect of fixed buffer is less than that shown in Fig. 11 A (c and d). The reason for this is that the time constant of decay of the STOC is independent of the magnitude of the $I_{Ca(spark)}$ (Fig. 10), and it corresponds to the mean open time of the BK channels in this preparation (Singer and Walsh, 1987). This appears to be in-

Published November 29, 2000

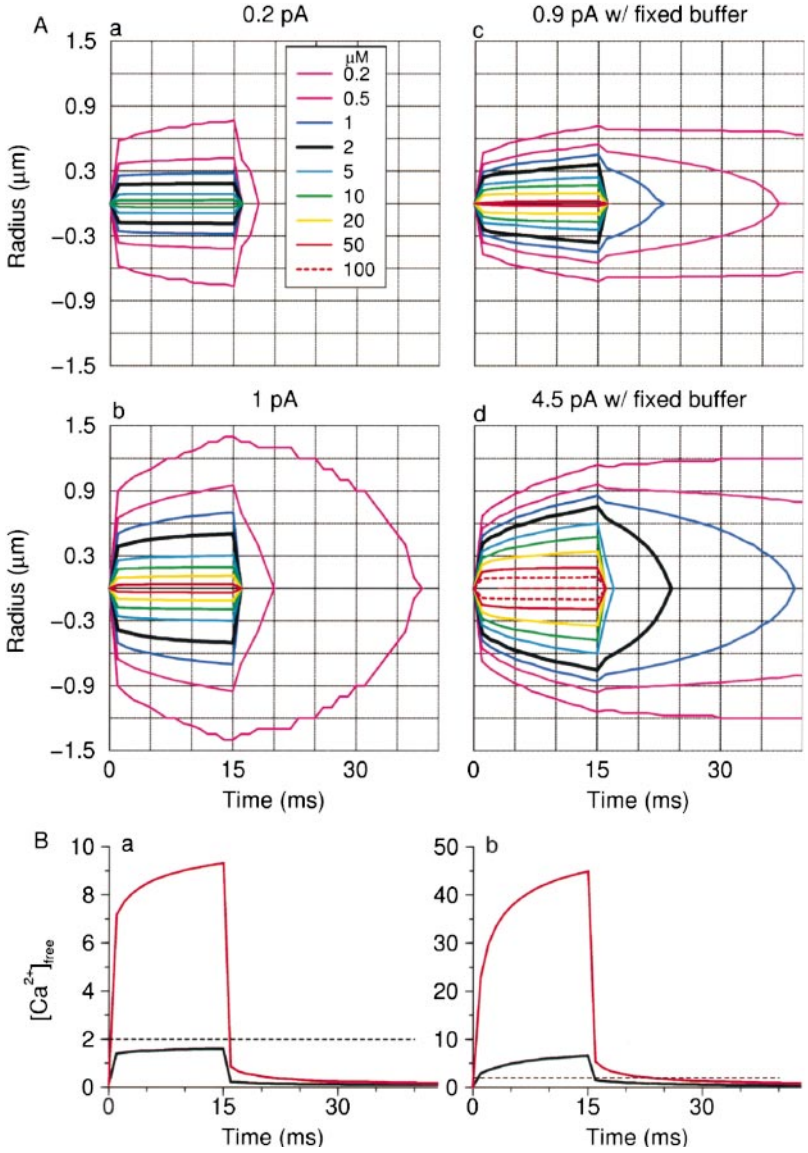

FIGURE 11. Simulations of spatiotemporal profile of Ca^{2+} concentration in response to a 15-ms pulse of Ca^{2+} current from a focal SR Ca^{2+} release site. Simulation of signal mass calculated from the total fluorescence in response to Ca^{2+} currents released from a focal SR source into the cytosol in the presence of 50 μM fluo-3 alone or in the presence of fixed buffer at a concentration of 230 μM, with a k_{on} of 10^{-8} $M^{-1}s^{-1}$ and k_{off} of 200 s^{-1}. See also Fig. 1. The Ca^{2+} currents used (0.2 and 1 pA in the absence of fixed buffer, and 0.9 pA and 4.5 pA in its presence) are based on measured values of the signal mass. In each case, the concentration changes shown result from a 15-ms pulse of Ca^{2+} current (not shown). (A) Spatiotemporal profiles of $[Ca^{2+}]$ in response to a 15-ms pulse of current of the magnitude indicated and with onset at time 0 in the absence (a, 0.2 pA; and b, 1 pA) and the presence (c, 0.9 pA; and d, 4.5 pA) of fixed buffer. (B) Time course of change in $[Ca^{2+}]$ at a fixed distance (200 nm) from the release site in response to a 15-ms pulse of Ca^{2+} current in the absence (a, black line for 0.2 pA; and red line for 1 pA) and the presence (b, black line for 0.9 pA; and red line for 4.5 pA) of fixed buffer. The dashed line indicates the $[Ca^{2+}]_{EC50}$ for the BK channels in excised patches at 0 mV.

compatible with a continued presence of substantial levels of Ca^{2+} at the offset of the current pulse as found with a fixed buffer of the type and concentration shown. Hence, the condition in the spark microdomain would seem to resemble more closely the conditions modeled in Fig. 11 A (a and b), where fixed buffer has relatively little effect and the main buffer is fluo-3.

DISCUSSION

In this paper, we have developed a new approach to the analysis of Ca^{2+} sparks. This approach takes its inspiration from the very perceptive work of Sun et al. (1998), but differs from it in that our approach is more direct. Sun et al. (1998) set out to determine the total Ca^{2+} (i.e., signal mass) released during a Ca^{2+} puff using confocal microscopy. To do so, they first estimated the $[Ca^{2+}]$ using the measured fluorescence, and then modeled the extent of the puff to obtain an estimate of signal mass (i.e., total Ca^{2+} released). Their starting point was an estimate of $[Ca^{2+}]$ since the confocal microscope is appropriate to make that measure in a restricted region. In contrast, we used a widefield system, with high spatiotemporal resolution and signal to noise ratio, to measure the signal mass directly by simply collecting the total increase in fluorescence over a sufficiently large region. The first derivative of the signal mass is the Ca^{2+} current or, when multiplied by a constant, the Ca^{2+} current flowing through RyRs at the spark site, $I_{Ca(spark)}$; and we have been able to make a measurement of this Ca^{2+} current. Because the measure of signal mass is direct, it is free from the necessity of 3-D modeling of the spark and the assumptions involved therein. Moreover, this approach provides a measure of the Ca^{2+} current through the RyRs under physiological conditions in the

Published November 29, 2000

cell with Ca^{2+} as the current carrier. Hence, this measure of $I_{Ca(spark)}$ provides a complement to measures of RyR currents recorded in bilayers.

Ca^{2+} Sparks Are due to the Concerted Opening of Multiple RyRs

It has been controversial whether the opening of a single RyR or the concerted opening of a cluster of multiple RyRs is responsible for a Ca^{2+} spark in smooth, cardiac, and skeletal muscle (Cheng et al., 1993; Lipp and Niggli, 1996; Blatter et al., 1997; Gollasch et al., 1998; Shirokova et al., 1998; Fill et al., 1999; Schneider, 1999; Shtifman et al., 2000). In the present study, we found a range of $I_{Ca(spark)}$ that varies by more than a factor of five; hence, we conclude that most sparks are due to the concerted opening of a number of RyRs. Mejia-Alvarez et al. (1999) recently measured single cardiac RyR channel currents in artificial bilayers under ionic conditions approximating the physiological and concluded that the current is $<$0.6 pA, probably on the order of 0.35 pA. Those values were for a lumenal free [Ca^{2+}] of $\sim$1 nM. Measurements of lumenal [Ca^{2+}] in the cells used here indicate a value on the order of 150 μM (ZhuGe et al., 1999), so we expect that the single RyR current in these cells is smaller than 0.35 pA, perhaps one tenth as small. The smallest mean $I_{Ca(spark)}$ that we detected is 0.15 or 0.23 pA. Do the smallest sparks arise from the opening of a single RyR? This remains uncertain. If the single-channel RyR Ca^{2+} currents in the cells used here are on the order of that seen by Mejia-Alvarez et al. (1999), then the smallest currents we found are likely due to a single RyR. If the single-channel currents are a tenth the value, then even the smallest sparks arise from a number of RyRs on the order of 10 and the largest ones from a number on the order of 50.

Clearance of Ca^{2+} Liberated by a Ca^{2+} Spark

One of the most striking features of the time course of the signal mass is the prolonged plateau once the peak of the signal mass is reached (Fig. 2). This plateau indicates that virtually all of the Ca^{2+} remains in the cytosol for the period of the plateau that is several times longer than the time to peak. This is consistent with what has been concluded for sparks in cardiac cells where diffusion accounts for $>$80% of the decay in fluorescence (Gomez et al., 1996). The plateau observed in the present study means that significant removal or sequestration of Ca^{2+} by pumps, exchangers, or entry into mitochondria does not occur after the termination of the Ca^{2+} current during the time of the plateau. Such removal would cause a decline rather than a plateau. If removal by these mechanisms is significant, it must occur during the rising phase of the signal mass. Hence, these Ca^{2+} removal mechanisms have a limited time to exert their effects, which, in turn, places constraints on their contribution. This fact may be pertinent when considering the existence and function of restricted spaces lying between SR and plasma membrane (Lederer et al., 1990; Van Breeman et al., 1995). The failure of removal mechanisms to exert a discernible effect during the time of the plateau is consistent with the low cytosolic concentrations of Ca^{2+} to be expected as Ca^{2+} quickly diffuses over an increasing volume with the dimensions of microns.

The Kinetics of STOCs

Although there is an extensive literature on STOCs, there is relatively little information on the kinetics of their rise and decay (Bolton and Imaizumi, 1996). Part of the reason for this may be that individual STOCs are somewhat noisy (Fig. 4). The signal averaging technique that we used here allowed us to examine the kinetics for groups of large and small STOCs (Fig. 9 C) as well as kinetics for groups of STOCs corresponding to large and small values of mean $I_{Ca(spark)}$ (Fig. 5 D). We found little variation in the kinetics of the rising phase, even with large differences in $I_{Ca(spark)}$ (Fig. 5). One interpretation of this data is that the BK channels are exposed to a high enough [Ca^{2+}] that their activation rate has reached a maximum, even when $I_{Ca(spark)}$ is relatively small. This would be the case if the BK channels lie close to the release site (See below).

The STOC decay was well fit by a single exponential with a time constant of 24–30 ms. This is in good agreement with the value of $\sim$30 ms for the effective mean open time at 0 mV for BK channels in excised patches from the same cells used here (Singer and Walsh, 1987). The activation rate for the STOCs is much faster, with time constants on the order of 3–4 ms for each of the independent subunits in the model used (Figs. 8 A and 4 C). Hence, if activating levels of Ca^{2+} persisted for a significant period of the decay period, the time of decay should be significantly longer than the mean open time. Therefore, it appears that the [Ca^{2+}] at the Ca^{2+} binding site of the BK channels drops rapidly (i.e., within a few milliseconds) upon termination of the Ca^{2+} current.

It is of interest to compare the kinetics of the STOCs with BK channels studied in other preparations. However, this is difficult because of the variability in the BK channel sensitivity to Ca^{2+}, due in part to the presence or absence of β subunits and perhaps other factors. Most appropriate for the present study is a comparison to the behavior of BK channels examined by Markwardt and Isenberg (1992) in excised inside-out patches from guinea pig urinary bladder smooth muscle cells. The work of Markwardt and Isenberg (1992) is most relevant to the present study since, to the best of our knowledge, it is the only report of the response of BK channels in excised patches to rapid concentration jumps of Ca^{2+}. It appears both from simulations of Ca^{2+} diffusion and from the conclusions drawn in the

Published November 29, 2000

previous paragraphs that during a spark the BK channels are exposed to a change in $[Ca^{2+}]$ that is more rapid than the BK channel kinetics. At the offset of a $[Ca^{2+}]$ jump at 0 mV, Markwardt and Isenberg find an exponential decay of BK channel activity with a time constant of 37 ms (Fig. 9 B in Markwardt and Isenberg, 1992) that is independent of $[Ca^{2+}]$ to which the channels were previously exposed. This result is in remarkably good agreement with our findings (Fig. 10). For the activation of the BK channels at the onset of a $[Ca^{2+}]$ jump, Markwardt and Isenberg (1992) used a Hodgkin-Huxley type of formulation to fit their data, based on three independent Ca^{2+} binding subunits. We used the same formulation to fit the time course of STOC activation, simply as a way of fitting the data to facilitate comparisons among the different groups of STOCs and with the experiments of Markwardt and Isenberg. Our data were well fit with time constants that did not vary systematically either with the amplitude of the STOC (Fig. 9 C) or with the amplitude of the $I_{Ca(spark)}$ (Fig. 5 D). We used time constants of ~3–4 ms which, in the work of Markwardt and Isenberg, resulted from a $[Ca^{2+}]$ jump in excess of 20 μM (Fig. 9 A in Markwardt and Isenberg, 1992). (Although those BK channels may be somewhat less sensitive to $[Ca^{2+}]$ than the ones underlying the STOCs in the present study [Fig. 7 in Markwardt and Isenberg, 1992 versus Fig. 6 in Singer and Walsh, 1987], the difference appears to be small.) Markwardt and Isenberg found that at jumps to $[Ca^{2+}]$'s in excess of 20 μM, where the kinetics of activation were fastest, the diffusion of Ca^{2+} to the patch within the pipet became rate limiting. The maximal $[Ca^{2+}]$ to which the BK channels can be exposed in our experiments is 150 μM, which is the free concentration measured in the SR of these cells (ZhuGe et al., 1999). Hence, it would appear that the BK channels are exposed to a $[Ca^{2+}]$ between 20 and 150 μM during a spark in the cells studied here, but experimental evidence is necessary to establish this point with certainty.

The Mechanism of STOC Generation by Ca^{2+} Sparks: Two Views

Two general views of STOC generation might be considered. In the first of these, the spark microdomain is simply the whole cell writ small. According to this view, the amplitude of the STOC is indicative of the level of submembranous $[Ca^{2+}]$; that is, with higher $[Ca^{2+}]$, the P_o of the BK channels is increased and the STOCs are larger. Hence, a relationship between $[Ca^{2+}]$ in the spark microdomain and STOC amplitude is to be expected. This view depends on several assumptions. First, the concentration of BK channels at each spark site must be the same. Second, the $[Ca^{2+}]$ to which the BK channels are exposed must be below saturating levels so that P_o is not always 1 during a spark. Third, there must be sufficient time during a spark for equilibrium to be achieved between the $[Ca^{2+}]$ and the channel, i.e., the BK kinetics must be relatively fast. Hence, according to this view, the rising phase of the STOC reflects the rise in $[Ca^{2+}]$ at the BK channels during the spark. In summary, this view does not need to take account of BK channel kinetics because the relationship between P_o and $[Ca^{2+}]$ at equilibrium explains the variability in STOC amplitude. In this case, the rise in $[Ca^{2+}]$ is the rate-limiting step, and the BK channels track this rise.

An alternative view emerging from the data presented here arises from the special properties of a microdomain where the RyR and the BK channels lie close together. If these two proteins are close enough, then the $[Ca^{2+}]$ will be sufficiently high in every case that the equilibrium P_o of the BK channels will always be one. Moreover, the $[Ca^{2+}]$ in this microdomain can reach a steady state level very quickly, too quickly for the BK channels to be in equilibrium as the $[Ca^{2+}]$ rises. On this view, the rise in the STOC and its decay reflect the BK channel kinetics as the $[Ca^{2+}]$ in the microdomain rises rapidly at the onset of the Ca^{2+} current and dissipates rapidly on its termination. In this case, the relationship between the Ca^{2+} current and the amplitude of the STOC will be largely independent of the magnitude of the $I_{Ca(spark)}$. However, the amplitude of the STOC for a given magnitude of the $I_{Ca(spark)}$ will vary depending on the density of the BK channels. And the STOC amplitude will increase the longer the duration of the $I_{Ca(spark)}$ since a greater fraction of BK channels will activate with time given their relatively slow kinetics. In this case, the BK channel kinetics are the rate-limiting factor after the rapid, switchlike changes in $[Ca^{2+}]$ from very low levels to saturating levels and back. The controlling factor is the ability of $[Ca^{2+}]$ to very rapidly reach a very high steady state level within the microdomain.

If this second view is correct, then why is there a relationship, however weak, between the Ca^{2+} signal mass and the magnitude of the STOC? First, the signal mass will be larger for Ca^{2+} currents of longer duration, and the STOC will continue to rise as long as the Ca^{2+} current persists until a P_o of one is reached. A second possible, though admittedly speculative, reason for the correlation between signal mass and STOC amplitude may be lie in the molecular architecture of the spark microdomain. One of the most striking findings in the present study is that the same Ca^{2+} current over the same period of time yields STOCs that vary several-fold in amplitude. The most straightforward interpretation of this result, given that the kinetics of the accompanying STOCs are the same, is that the ratio of RyRs to BK channels varies from spark site to spark site. One way to account for this is to postulate two types of RyRs, one type linked to BK channels and another type not linked. In this way, there is a constant proportionality

between RyRs of the first type and BK channels, but this proportionality will be weakened by RyRs of the second type. In this way, a weak correlation will emerge between spark signal mass and STOC amplitude. One interesting feature of this sort of mechanism is that it suggests a physical linkage, direct or indirect, between RyRs and BK channels reminiscent of the link between RyRs and L-type Ca^{2+} channels in skeletal muscle.

We would like to thank Ian Parker, Karl Magleby, Michael Stern, Michael Kirber, and Catherine O'Reilly for their thoughtful reading of the manuscript and helpful comments and discussion. We thank Jeffrey Carmichael, Rebecca McKinney, and Paul Tilander for excellent technical assistance, and Stephen Baker for help with the statistical analysis.

This study was supported by a grant from the National Institutes of Health (HL 61297-01) and grants from the National Science Foundation (DBI-9724611 and DIR9200027).

Submitted: 19 September 2000
Revised: 24 October 2000
Accepted: 25 October 2000

REFERENCES

Blatter, L.A., J. Huser, and E. Rios. 1997. Sarcoplasmic reticulum Ca^{2+} release flux underlying Ca^{2+} sparks in cardiac muscle. *Proc. Natl. Acad. Sci. USA.* 94:4176–4181.

Bolton, T.B., and Y. Imaizumi. 1996. Spontaneous transient outward currents in smooth muscle cells. *Cell Calcium.* 20:141–152.

Bolton, T.B., and D.V. Gordienko. 1998. Confocal imaging of calcium release events in single smooth muscle cells. *Acta Physiol. Scand.* 164:567–575.

Bond, M., H. Shuman, A.P. Somlyo, and A.V. Somlyo. 1984. Total cytoplasmic calcium in relaxed and maximally contracted rabbit portal vein smooth muscle. *J. Physiol.* 357:185–201.

Brenner, R., G.J. Perez, A.D. Bonev, D.M. Eckman, J.C. Kosek, S.W. Wiler, A.J. Patterson, M.T. Nelson, and R.W. Aldrich. 2000. Vasoregulation by the β1 subunit of the calcium-activated potassium channel. *Nature.* 407:870–876.

Carrington, W.A., R.M. Lynch, E.D.W. Moore, G. Isenberg, K.E. Fogarty, and F.S. Fay. 1995. Superresolution three-dimensional images of fluorescence in cells with minimal light exposure. *Science.* 268:1483–1487.

Cheng, H., W.J. Lederer, and M.B. Cannell. 1993. Calcium sparks: elementary events underlying excitation-contraction coupling in heart muscle. *Science.* 262:740–744.

Collier, M.L., G. Ji, Y.-X. Wang, and M.I. Kitlikoff. 2000. Calcium-induced calcium release in smooth muscle: loose coupling between the action potential and calcium release. *J. Gen. Physiol.* 115:653–662.

Drummond, R.M., and F.S. Fay. 1996. Mitochondria contribute to Ca^{2+} removal in smooth muscle cells. *Pflügers Arch.* 431:473–482.

Fay, F.S., R. Hoffman, S. Leclair, and P. Merriam. 1982. Preparation of individual smooth muscle cells from the stomach of *Bufo marinus. Methods Enzymol.* 85:284–291.

Fill, M., P. Mejia-Alvarez, C. Kettlun, and A. Escobar. 1999. Ryanodine receptor permeation and gating: glowing cinders that underlie the Ca^{2+} spark. *J. Gen. Physiol.* 114:159–161.

Gollasch, M., G.C. Wellman, H.J. Knot, J.H. Jaggar, D.H. Damon, A.D. Bonev, and M.T. Nelson, 1998. Ontogeny of local sarcoplasmic reticulum Ca^{2+} signals in cerebral arteries. Ca^{2+} sparks as elementary physiological events. *Circ. Res.* 83:1104–1114.

Gomez, A.M., H. Cheng, W.J. Lederer, and D.M. Bers. 1996. Ca^{2+} diffusion and sarcoplasmic reticulum transport both contribute to $[Ca^{2+}]_i$ decline during Ca^{2+} sparks in rat ventricular myocytes. *J. Physiol.* 496:575–581.

Harkins, A.B., N. Kurebayashi, and S.M. Baylor. 1993. Resting myoplasmic free calcium in frog skeletal muscle fibers estimated with fluo-3. *Biophys. J.* 65:865–881.

Kargacin, G., and F.S. Fay. 1991. Ca^{2+} movement in smooth muscle cells studied with one- and two-dimensional diffusion models. *Biophys. J.* 60:1088–1100.

Kirber, M.T., K.D. Bellve, L.M. Lifshitz, R.A. Tuft, J.V. Walsh Jr., and K.E. Fogarty. 1998. High speed 3-D imaging reveals differences between sparks that generate STOCs and those that do not. *Biophys. J.* 74:272. (Abstr.)

Lederer, W.J., E. Niggli, and R.W. Hadley. 1990. Sodium-calcium exchange in excitable cells: fuzzy space. *Science.* 248:4953–4955.

Lipp, P., and E. Niggli. 1996. Submicroscopic calcium signals as fundamental events of excitation-contraction coupling in guinea-pig cardiac myocytes. *J. Physiol.* 492:31–38.

Markwardt, F., and G. Isenberg. 1992. Gating of maxi K^+ channels studied by Ca^{2+} concentration jumps in excised inside-out multichannel patches (myocytes from guinea pig urinary bladder). *J. Gen. Physiol.* 99:841–862.

Mejia-Alvarez, P., R.C. Kettlun, E. Rios, M.D. Stern, and M. Fill. 1999. Unitary Ca^{2+} currents through cardiac ryanodine receptors under quasi-physiological ionic conditions. *J. Gen. Physiol.* 113:177–186.

Mironneau, J., S. Arnaudeau, N. Macrez-Lepretre, and F.X. Boittin. 1996. Ca^{2+} sparks and Ca^{2+} waves activate different Ca^{2+}-dependent ion channels in single myocytes from rat portal vein. *Cell Calcium.* 20:153–160.

Naraghi, M., and E. Neher. 1997. Linearized buffered Ca^{2+} diffusion in microdomains and its implications for calculation of $[Ca^{2+}]$ at the mouth of a calcium channel. *J. Neurosci.* 17:6961–6973.

Nelson, M.T., H. Cheng, M. Rubart, L.F. Santana, A.D. Bonev, H.J. Knot, and W.J. Lederer. 1995. Relaxation of arterial smooth muscle by calcium sparks. *Science.* 270:633–637.

Pabelick, C.M., Y.S. Perkash, M.S. Kannan, and G.C. Sieck. 1999. Spatial and temporal aspects of calcium sparks in porcine tracheal smooth muscle cells. *Am. J. Physiol.* 277:L1018–L1025.

Parker, I., and Y. Yao. 1991. Regenerative release of calcium from functionally discrete subcellular stores by inositol trisphosphate. *Proc. R. Soc. Lond. B. Biol. Sci.* 246:269–274.

Perez, G.J., A.D. Bonev, J.B. Patlak, and M.T. Nelson.1999. Functional coupling of ryanodine receptors to K_{Ca} channels in smooth muscle cells from rat cerebral arteries. *J. Gen. Physiol.* 113:229–237.

Robertson, S.P., J.D. Johnson, and J.D. Potter. 1981. The time-course of Ca^{2+} exchange with calmodulin, troponin, parvalbumin, and myosin in response to transient increase in Ca^{2+}. *Biophys. J.* 34:559–569.

Schneider, M.F. 1999. Ca^{2+} sparks in frog skeletal muscle: generation by one, some, or many SR Ca^{2+} release channels? *J. Gen. Physiol.* 113:365–371.

Shirokova, N., J. Garcia, and E. Rios. 1998. Local calcium release in mammalian skeletal muscle. *J. Physiol.* 512:377–384.

Shtifman, A., C.W. Ward, J. Wang, H.H. Valdivia, and M.F. Schneider. 2000. Effects of iperatoxin A on local sarcoplasmic reticulum Ca^{2+} release in frog skeletal muscle. *Biophys. J.* 79:814–827.

Singer, J.J., and J.V. Walsh Jr. 1987. Characterization of calcium-activated potassium channels in single smooth muscle cells using the patch-clamp technique. *Pflügers Arch.* 408:98–111.

Smith, G.D., J.E. Keizer, M.D. Stern, W.J. Lederer, and H. Cheng. 1998. A simple numerical model of calcium spark formation and detection in cardiac myocytes. *Biophys. J.* 75:15–32.

Stern, M.D. 1992. Buffering of calcium in the vicinity of a channel pore. *Cell Calcium.* 13:183–192.

Published November 29, 2000

Sun, X.P., N. Callamaras, J.S. Marchant, and I. Parker. 1998. A continuum of $InsP_3$-mediated elementary Ca^{2+} signalling events in *Xenopus* oocytes. *J. Physiol.* 509:67–80.

Thomas, D., P. Lipp, M.J. Berridge, and M.D. Bootman. 1998. Hormone-evoked elementary Ca^{2+} signals are not stereotypic, but reflect activation of different size channel clusters and variable recruitment of channels within a cluster. *J. Biol. Chem.* 273:27130–27136.

Van Breeman, C., Q. Chen, and I. Laher. 1995. Superficial buffer barrier function of smooth muscle sarcoplasmic reticulum. *Trends Pharmacol. Sci.* 16:98–104.

ZhuGe, R., S.M. Sims, R.A. Tuft, K.E. Fogarty, and J.V. Walsh Jr. 1998. Ca^{2+} sparks activate K^+ and Cl^- channels, resulting in spontaneous transient currents in guinea pig tracheal myocytes. *J. Physiol.* 513:711–718.

ZhuGe, R., R.A. Tuft, K.E. Fogarty, K. Bellve, F.S. Fay, and J.V. Walsh Jr. 1999. The influence of sarcoplasmic reticulum Ca^{2+} concentration on Ca^{2+} sparks and spontaneous transient outward currents in single smooth muscle cells. *J. Gen. Physiol.* 113:215–228.

Zou, H.L., M. Lifshitz, R.A. Tuft, K.E. Fogarty, and J.J. Singer. 1999. Imaging Ca^{2+} entering the cytoplasm through a single opening of a plasma membrane cation channel. *J. Gen. Physiol.* 114:575–588.